LASER LITHOGRAPHY OF DIBLOCK COPOLYMER FILMS

LASER LITHOGRAPHY OF DIBLOCK COPOLYMER FILMS

By

JOSEPH PARETE
B. Eng. Mgmt. (McMaster) 2006

A Thesis
Submitted to the School of Graduate Studies
in Partial Fulfillment of the Requirements
for the Degree
Master of Applied Science

McMaster University
©Copyright by Joseph Parete, September 2008

MASTER OF APPLIED SCIENCE (2008)
(Engineering Physics)

McMaster University
Hamilton, Ontario

TITLE: Laser Lithography of Diblock Copolymer Films
AUTHOR: Joseph Parete, B. Eng. Mgmt. (McMaster University)
SUPERVISORS: Dr. John S. Preston and Dr. Kari Dalnoki-Veress
NUMBER OF PAGES: xii, 75

Abstract

Laser lithography was used to create novel patterns in thin diblock copolymer films. These patterns were characterized and an examination of their formation and growth was conducted. The patterns occurred only in diblock films, due to the interaction between thermal gradient induced Marangoni flow and the self assembly of the molecules. Growth of the patterns was found to be strongly dependent on absorbed power. The impact of film thickness on pattern growth was mainly due to the corresponding changes in sample reflectance, however a periodic patterning was observed suggesting that growth is also dependent on the amount of 'excess' material (over that required to form complete lamella) available. It was also shown that the pattern growth can occur independently of laser lithography and the Marangoni effect, though laser lithography was required to direct this growth.

Preface

After reading the following list of thanks, you may wonder what part I had in completing this thesis. While it is true that my name is on the cover, this work would never have existed without the support of a group of people to which I owe my deep gratitude.

I'd like to start by thanking my supervisors, Dr. John Preston and Dr. Kari Dalnoki-Veress. John, you were the one who gave me my first real taste of a research environment, and I cannot thank you enough for your constant support, encouragement and guidance throughout the years. Kari, working with you has been a real honour and pleasure. I will always appreciate both the confidence you've shown in me and the enthusiasm you've had in support of this work.

I would also like to thank all of my fellow lab members throughout the past few years. You've all made it a pleasure to work and study here at McMaster, and I look back on these years with nothing but fond memories. To Rob, John, John, Mike, Andrew, Adam, Marie-Josée, Jessica, Josh, Marc-Antoni, and all of the summer students past and present: Thank you. I'd like to particularly thank John Hudson for his pioneering work on laser lithography, Mike Massa for his continued assistance on all matters lab-y, and Andrew Croll for his insight into the mysterious diblock copolymer.

Lastly, I'd like to thank all of my friends (you know who you are...) and family, especially my mother, father and sister. I know that I may not have always expressed this, but have no doubt that when times were tough, you were the light that helped me find my way.

JOSEPH PARETE
SEPTEMBER 2008

Contents

List of Figures **ix**

List of Tables **xi**

1 Introduction **1**

1.1 The Lithographic Process - Past and Present 1

1.2 Polymers 3

1.2.1 Diblock Copolymers 5

1.3 Laser Lithography of Thin Polymer Films 12

1.3.1 Surface Tension and the Marangoni Effect 12

1.3.2 Laser Induced Heating 14

1.3.3 Fluid Flow Profile 17

2 Experimental Details **21**

2.1 Sample Preparation 21

2.1.1 Spin Casting 22

2.1.2 Flow Coating 23

2.2 Sample Processing 26

2.2.1 Optical Systems 27

2.2.2 Software Control 34

2.3 Sample Characterization 37

2.3.1 Optical Microscopy 39

2.3.2 Atomic Force Microscopy 41

3 Results and Discussion 43
3.1 Observed Behavior 43
3.2 Effects of Parameter Variation on Patterning 46
    3.2.1 Film Composition 46
    3.2.2 Scan Velocity 48
    3.2.3 Laser Power 50
    3.2.4 Film Thickness 53
    3.2.5 Temperature 58

4 Conclusions 61

Bibliography 65

Appendices 71

A Laser Specifications 71

B Spot Size Calculation 73

C Backlash Correction Algorithm 75

List of Figures

1.1 The 'Chain' Picture of Polymers 4
1.2 Homopolymer Architectures 6
1.3 Block Copolymer Architectures 6
1.4 Diblock Segregation 7
1.5 Symmetric Diblock Microphase Separation 8
1.6 Diblock Microphase Separation 9
1.7 Ordered Symmetric Diblock on a Substrate 9
1.8 A Depiction of Surface Tension 13
1.9 A Depiction of Variations in Surface Tension 13
1.10 Marangoni Forces on Surface Molecules 14
1.11 Reflectance of 532 nm Light from P(S-b-MMA) Thin Films . . 16
1.12 Velocity Profile in a Sheared Newtonian Fluid 18
1.13 Material Flow in a Locally Heated Film 18
1.14 AFM Image of a Patterned 'Trench' and 'Crater' 19

2.1 Flow Coating Schematic 24
2.2 Flow Coater Velocity Profiles 26
2.3 Optical System - Section A 28
2.4 Function of the Polarizing Beamsplitter 29
2.5 Optical System - Section B 31
2.6 Flow Diagram of the Controlling LABVIEW Program 35
2.7 Examples of Various Patterns 38
2.8 Results of Contrast Adjustment 40
2.9 Optically Measurable Thickness Variations 40

2.10 Schematic Diagram of an Atomic Force Microscope 42

3.1 Comparison of Homopolymer and Diblock Patterns 44
3.2 Example of Patterned Diblock Copolymer Film 45
3.3 A View of Pattern 'Ends' 45
3.4 Pattern Formation in Various Polymers 47
3.5 Period as a Function of Scan Velocity 49
3.6 Pattern Period as a Function of Laser Power 51
3.7 Schematic Diagram of Two Islands Merging 52
3.8 Pattern Period as a Function of Laser Power and Film Thickness 53
3.9 Scaled Reflectivity of Samples 55
3.10 Pattern Period as a Function of Normalized Power and Thickness 56
3.11 'Knee Position' as a Function of Scaled Thickness 57
3.12 Pattern Formation at Various Powers and Temperatures . . . 58
3.13 Temperature Profile of Annealing Step 59
3.14 Post-Anneal Patterns 60

C.1 Flow Diagram of the Backlash Correcting Routine 75

List of Tables

1.1 Optical Properties of Relevant Materials 15

3.1 Pattern Formation in Various Polymers 48

A.1 Laser Specifications 71

Chapter 1

Introduction

1.1 The Lithographic Process - Past and Present

For many years, lithography has been an invaluable technique in transferring patterns from one surface to another. The word itself, which comes from the Greek words for 'stone' (*lithos*) and 'writing' (*graphia*), indicates the origin of this technique. It was invented by Aloys Senefelder in 1796 as a method to transfer an image from a relatively smooth piece of limestone onto a piece of paper [1]. This method of printing is still used today, though in modern times, the term 'lithography' has taken on a broader meaning. Still, though, in the context of this thesis, lithography refers to the printing of a pattern onto a substrate.

Perhaps the most well known technological adaptation of this technique is in *photolithography*. Photolithography is a technique used to transfer a pattern from a patterned metal film (a "mask") to thin films on technologically relevant substrates (for example, silicon). Basically, photolithography involves coating a substrate with a light sensitive polymer, and exposing this polymer to light through a mask. Exposed areas will be chemically modified by the light, allowing the selective removal of either the exposed or unexposed regions of polymer. The net result of this process is that the mask pattern is transferred, or printed, into the polymer layer, allowing for subsequent processing (i.e. removal) of the exposed substrate.

Photolithography has become a critical component of the fabrication of microelectronic circuits, and as such, has been the focus of intense research. This research has increased both the resolution and the flexibility of the technique, enabling the creation of smaller features in more varied materials. Despite its widespread use, however, photolithography does have limitations that prevent it from being applicable in all situations. Two such limitations are the speed at which different patterns can be made and the resolution of the printing process.

Due to the fact that patterns are created in parallel by exposing an entire mask to light, photolithography excels at high speed reproduction of any given pattern for which a mask is available. However, since the only pattern that can be created is that found on the mask, the only way to modify a pattern is to produce a new mask; typically an expensive, time consuming process. This makes photolithography ill-suited to the rapid prototyping of devices. An alternative to the parallel exposure of photolithography is to *directly write* patterns into thin films. If photolithography can be compared to 'stamping' a pattern onto a film, 'direct-write' methods can be compared to writing a pattern with a pencil. Though they are perhaps an abuse of the meaning of the word 'lithography', these methods allow for the serial creation of features. As direct write systems are typically controlled by a computer that scans a tightly focused beam across a sample, no physical mask is needed [1]. Thus, changing a pattern is as simple as changing the parameters of the control software, a relatively simple modification. Though their serial nature makes the production of many copies of a given pattern impractical, direct write techniques, of which laser lithography is one, are well suited to the creation of few numbers of specialized and variable patterns.

A second limitation of photolithography is the resolution of the patterns, often expressed as a minimum produceable feature size. As photolithography is a fundamentally optical technique, it is no surprise that its resolution is limited by the diffraction of light. As a general guideline, the minimum feature size scales with the wavelength of light being used. A main focus of research has thus been to find light sources and light sensitive materials for smaller and smaller wavelengths. Over many years, this has led from visible light exposure to ultraviolet light exposure, with x-ray exposure as a possible future goal [2]. There are, however, other ways of producing patterns with very small features. One of the most interesting of these is to use materials that assemble themselves into patterns on nanoscopic length scales. Indeed, one of the promising themes within the development of nanotechnology is the combination of self-assembly with conventional micro-patterning techniques [3, 4]. Block copolymers are an example of a material with the ability to self assemble, and will be the focus of this research. Before block copolymer can be discussed, however, is is essential to have a grasp on what polymers themselves are.

1.2 Polymers

Polymers are commonly found in nature, and include such materials as rubbers, proteins and DNA. Their unique properties make them so well suited to technological applications that synthetic polymers have become ubiquitous in modern society. Examples of common synthetic polymers include polyethylene and polystyrene among others, and are employed everywhere from plastics to detergents to food additives. As with photolithography, the definition of a polymer can be inferred from the origin of the word. Polymers, from the Greek words for 'many' (*polloi*) and 'part' (*meros*) are molecules that consist of a large number of repeating units. These repeat units, referred to as 'monomers', are typically small molecules that are covalently bonded together to form extended structures. Perhaps the simplest example of a polymer is that of a linear homopolymer chain. An example of such a polymer, polyethylene, is illustrated in figure 1.1.

Due to their large number of individual components, statistical methods can and must be employed to successfully study such molecules. For many purposes, a coarse grained approach can be used which neglects the detailed

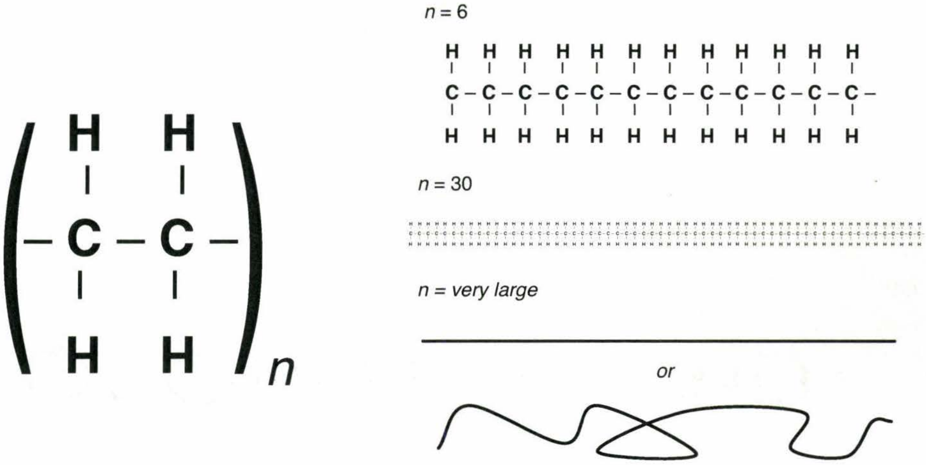

Figure 1.1: The 'chain' picture of polymers. An ethylene structural unit is shown on the left. By covalently bonding more and more of these molecules together, we obtain a structure that resembles a one-dimensional chain.

chemical structure of the polymer, and instead considers only its overall architecture. The statistical methods are based on the concept that the polymer chain is executing a random walk though space.

The origin of the random walk model for polymers can be discussed in the following way. As illustrated in figure 1.1, a simple linear polymer chain has a backbone of atoms (in this case, carbon) upon which side groups are attached. The backbone is held together by carbon-carbon bonds, which preferentially form at specific angles. The result is a short range order to the chain. However, though the bond angle is fixed in two dimensions, it is free to rotate along the 'axis' of the backbone. After a few atoms in the 'chain' have been added, this random rotation results in a loss of any correlation between two points along the chain. By 'coarse graining' the polymer, and considering the length of chain needed to lose this correlation (known as b) as one "statistical segment", the entire chain can be treated as a random walk of N steps, each having a length of b. As a result, the simple mathematical description of a random walk can be employed to predict chain behavior [5].

A key result that emerges from this treatment is the effective 'size' of a polymer chain. Though the contour length of a chain can be calculated by the product of the number of steps, N, and the step length, b, a more useful descriptor of the size of the chain is the distance between its two endpoints. This end-to-end vector, or **R**, is defined as the vector sum of all N steps taken along the polymer chain:

$$\mathbf{R} = \sum_{n=1}^{N} \mathbf{r}_n. \tag{1.1}$$

The square root of the scalar product of this vector with itself gives the length of the vector, in this case, the end-to-end distance of the polymer chain, R_{ee}. As there is no correlation between segments of a random walk, the sum of all cross terms is zero, giving a value for R_{ee} that depends simply on the number of steps, N, and the length of each step, b: [5]

$$R_{ee} = \sqrt{<\mathbf{R} \cdot \mathbf{R}>} = \sqrt{Nb^2}. \tag{1.2}$$

1.2.1 Diblock Copolymers

While the specific details of the polymer's chemical composition can often be neglected when considering the physics of a polymer chain, the same cannot be said for the polymer's architecture. Though a simple linear chain is the most common example, figure 1.2 illustrates some of the wide variety of architectures that are possible. Note that the illustrated polymers are "homopolymers", in that they are composed of only one type of monomer.

One important case is when different chemical species make up a single polymer chain. These types of polymers are known as heteropolymers or copolymers. More specifically, block copolymers are copolymers whose various segments are grouped into "blocks", which are then joined together into a larger polymer chain. Figure 1.3 illustrates several types of copolymers.

The molecules of particular interest for the laser lithography experiments discussed in this thesis are *diblock copolymers*. Diblock copolymers consist of two types of monomers grouped into blocks and covalently bonded to each other. Figure 1.3 illustrates a diblock copolymer. Copolymers in general, and

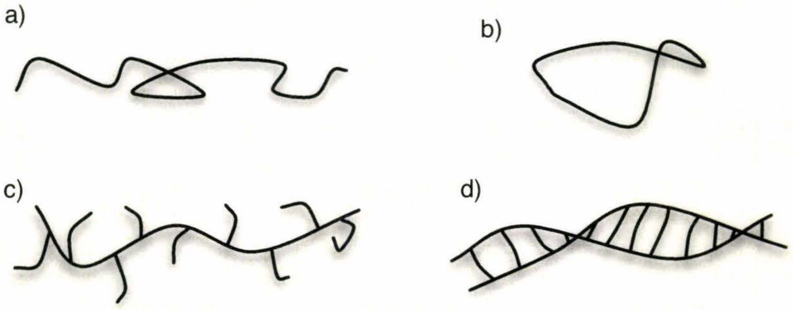

Figure 1.2: Homopolymer architectures. Four examples are illustrated: a) Linear Chain, b) Ring, c) Branched Ladder, and d) Branched Chain.

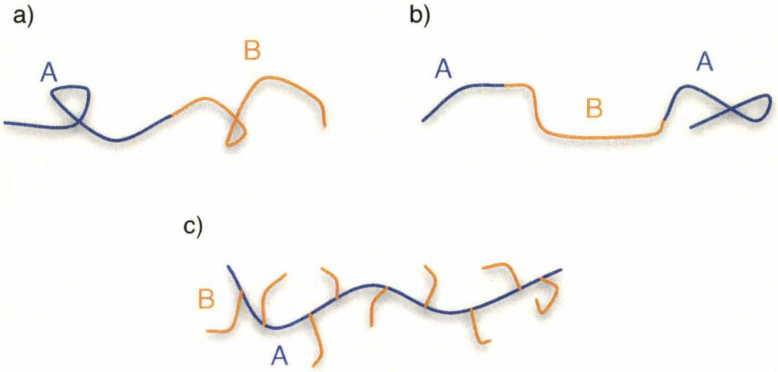

Figure 1.3: Block copolymer architectures. These are composed of two different monomer types, 'A' (in blue) and 'B' (in orange). Three examples are illustrated: a) Diblock Copolymer, b) Triblock Copolymer, c) Graft Copolymer.

block copolymers in particular, have the ability to self assemble into interesting structures. This ability can be understood by examining the interaction between the types of monomers that make up the polymer chain. Perhaps the simplest example is a *symmetric* diblock copolymer consisting of equally sized 'A' and 'B' blocks. The strength of the interaction between the 'A' and 'B' sections of the polymer can be characterized by the product of an "interaction parameter", χ^1, and the degree of polymerization (i.e. the number of monomers in a block), N.

If the 'A' monomers and the 'B' monomers were chemically identical, χ would be zero, meaning that χN would also be zero. In this case, we would have no segregation (or separation) of the two blocks. The diblock copolymer would be, in effect, a homopolymer with a degree of polymerization $2N$. For chemically dissimilar monomers, χ is nonzero, and typically represents repulsive interactions between the monomers. In this case, the degree to which the two blocks separate depends on the magnitude of χN. If $\chi N \sim 10.5$, the blocks are weakly segregated, while if $\chi N \gg 10$, the blocks would be strongly segregated [6]. Figure 1.4 illustrates these three regimes.

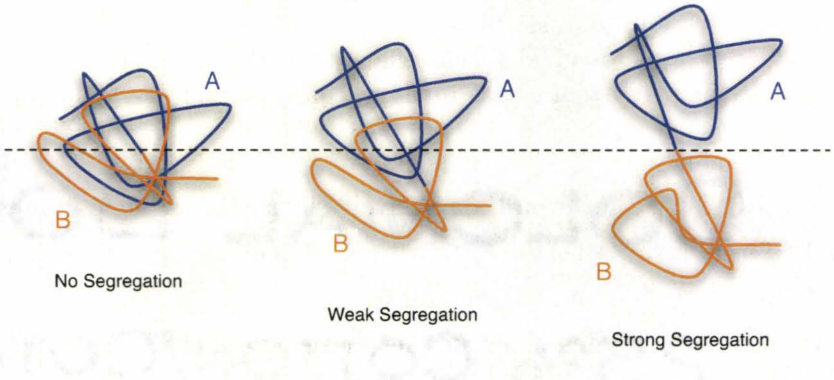

Figure 1.4: Diblock segregation. A comparison between unsegregated, weakly segregated, and strongly segregated diblock copolymers.

---

[1] χ is the Flory-Huggins interaction parameter. For most monomer-monomer interactions, χ is positive, indicating repulsion.

As seen in both the weakly and strongly segregated regimes, diblock copolymers with a positive χ tend to arrange themselves in such a way so as to minimize the unfavorable (repulsive) interaction. The more unfavorable the interaction, the stronger is the drive towards phase separation. Under "normal" circumstances, the polymers would phase separate into 'A' and 'B' rich regions on a macroscopic scale. However, since each polymer molecule has both 'A' and 'B' regions, and since these regions are covalently bound together, the polymer must instead demix by phase separation on a microscopic scale. This is achieved by each polymer molecule arranging itself with respect to its neighbors so as to minimize the unfavorable 'A' - 'B' interaction. As illustrated in figure 1.5, the result for symmetric diblock copolymers is a self assembly into layers (or lamella) of 'A' and 'B' rich regions.

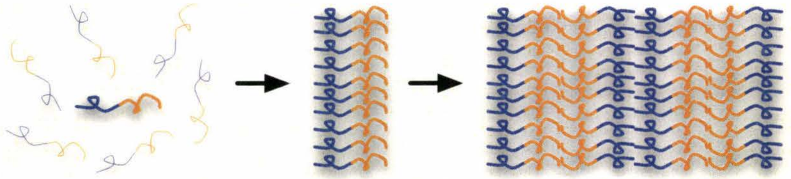

Figure 1.5: Symmetric diblock microphase separation. Symmetric diblocks that are unorganized (left) will self-assemble into lamella to minimize unfavorable 'A' - 'B' interactions (centre). Individual lamella will arrange themselves back to back (right) in order to produce a system with a minimum of interfacial energy.

Figure 1.6 shows that even the relatively simple diblock copolymer can self assemble into in a rich variety of structures, depending on the relative sizes of the 'A' and 'B' blocks, and the magnitude of χN.

In the experiments described in this thesis, symmetric diblock copolymer thin films on silicon substrates were used. In this case, a disordered film is formed on the substrate that, given the opportunity to do so, would self-assemble into lamella parallel to the surface of the substrate (figure 1.7).

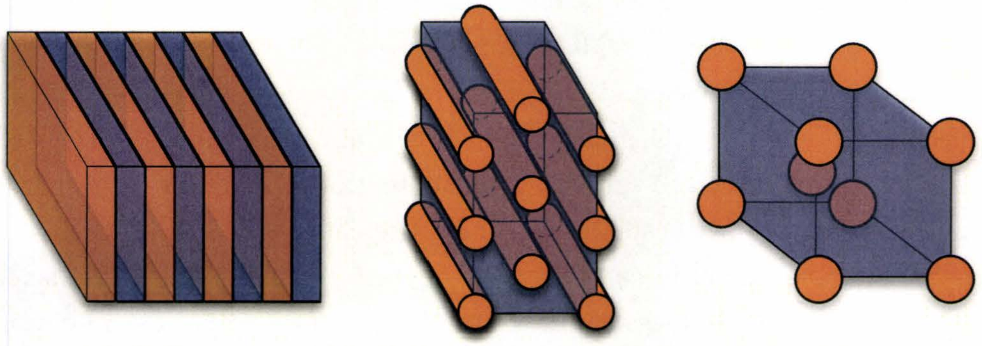

Figure 1.6: Diblock microphase separation. Depending on the interaction parameter, χN, and the relative sizes of the 'A' and 'B' blocks, a wide variety of structures can be formed by microphase separation. These include the lamellar, cylindrical, and spherical phases. [7]

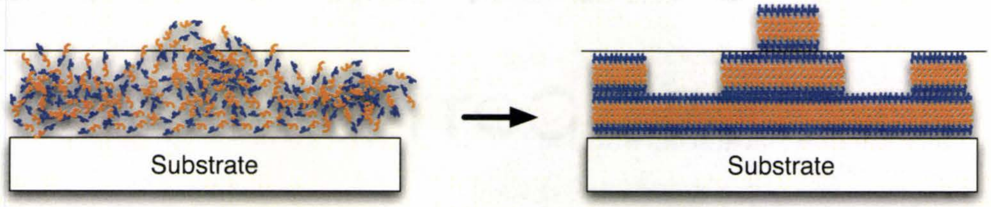

Figure 1.7: Ordered symmetric diblock on a substrate. The transition from a disordered to an ordered state for a symmetric diblock copolymer results in the formation of lamella.

Calculation of Lamellar Thickness

The thickness of the lamella formed by symmetric diblock copolymers that are strongly segregated can be calculated by examining the free energy of the system [6, 8, 9]. On the one hand, increasing lamellar thickness will decrease the amount of interface and so reduce the interfacial energy cost for a given volume of material. This effect, which can also be described as enthalpic repulsion, would tend to cause the lamella to grow in thickness. On the other hand, lamellar growth can only occur by stretching the polymer chains. The subsequent reduction in entropy would tend to resist any thickness increase. The equilibrium thickness can be found by minimizing the free energy from these two effects.

$$F_{total} = F_{interface} + F_{stretching} \tag{1.3}$$

As shown by Semenov [10], given a spacing of d, a statistical segment length of a, and N segments, the stretching contribution per chain is given by

$$\frac{F_{stretching}}{kT} \sim \frac{d^2}{a^2N}. \tag{1.4}$$

Further, the interfacial contribution per chain is the product of the interfacial tension, γ, and the area per chain, σ. Defining χ as the Flory-Huggins interaction parameter, these quantities are well known as [11]

$$\gamma \sim \frac{\chi^{1/2}}{a^2} \qquad \text{and} \qquad \sigma \sim \frac{Na^3}{d}. \tag{1.5}$$

Thus, the interfacial contribution for the free energy per chain is

$$\frac{F_{interface}}{kT} \sim \frac{\chi^2 Na}{d}. \tag{1.6}$$

The total free energy from both chain stretching and interfaces is therefore

$$\frac{F_{total}}{kT} = \frac{d^2}{a^2N} + \frac{Na\chi^{1/2}}{d}. \tag{1.7}$$

The equilibrium lamellar thickness can then be found by minimizing the sum of these contributions (equation 1.7) with respect to d, giving

$$d \sim a\chi^{1/6}N^{2/3}. \tag{1.8}$$

In order to calculate lamellar thicknesses, a prefactor is required. As developed by Semenov [12], including the prefactor, lamellar thickness is given by

$$d \simeq 2(3/\pi^2)^{1/3}a\chi^{1/6}N^{2/3}. \tag{1.9}$$

For an 18 kg/mol - b - 18 kg/mol sample of poly(styrene - b - methyl methacrylate), each of these parameters can be estimated. The parameter a can be taken to be approximately 0.67 nm [8]. χ is temperature dependent, given by the expression $\chi = 0.028 + 3.9/T$ [13]. For a typical processing temperature of 130 ℃, χ is approximately 0.038. Finally, knowing the molecular weight of styrene and methyl methacrylate, we can calculate that the entire molecule consists of 353 segments [14]. Using these values, the lamellar thickness is found to be approximately 26 nm.

The preceding calculation assumes that the diblock molecules are strongly segregated. However, in our case, χN is roughly 13, indicating weak segregation. Calculating lamellar thickness in this case is much more difficult, and requires a numerical solution to a self-consistent field theory (SCFT) [15].

Confirming the results of these calculations is as simple as measuring the exact lamellar thickness of the polymer in question. This has been done for our 18k - b - 18k PS-b-PMMA polymer, with the result of a lamellar period of approximately 29 ± 2 nm [14]. It is important to note the distinction between a lamellar period and a lamellar thickness. The thickness of a lamella is defined by the "length" of a diblock molecule while it is in an ordered state. However, as shown in in figure 1.5, lamella stack back-to-back. As a result, a lamellar *period* is equal to two lamellar thicknesses.

Reviewing our results, we see that if the polymer were strongly segregated, a lamellar period of 52 nm would be expected (twice the calculated lamellar thickness). Since we have weak segregation, however, we would expect thinner lamella. This is in fact the case, as shown by the measured value of 29 nm for lamellar period. One lamellar thickness is half this value, or approximately 14.5 nm.

1.3 Laser Lithography of Thin Polymer Films

At the core of the experiments described in this thesis is the laser lithography process itself. Originally developed for use with homopolymer films [19], it has been applied to diblock copolymer films with very interesting results. This section briefly describes the physical principles behind the laser lithography process, including surface tension and the thermally induced Marangoni effect.

1.3.1 Surface Tension and the Marangoni Effect

Surface tension is a general property of condensed matter. It arises at interfaces due to the differing interaction effects that atoms and molecules experience there. As an example, take the surface of a liquid that is exposed to air, as generally depicted in figure 1.8. Molecules of the liquid are depicted as circles, with the liquid-air interface represented by the dark line. A molecule on the 'inside' of the fluid (labelled 'B') experiences attractive interactions with other molecules in its vicinity. As it is surrounded by these molecules, the net force on 'B' is zero. Though also experiencing attractive interactions with its neighbors, a molecule at the interface (labelled 'A') is not surrounded. It thus experiences a net force inwards. This inward force is experienced by all molecules at the interface, and is the source the surface 'tension'.

An interesting effect occurs when there are variations in surface tension across a given volume of material. A variation in surface tension has the potential to cause the material to flow. To illustrate, figure 1.9 again schematically shows molecules near an interface. This time, the interactions between 'A' and its neighbors have been weakened, producing a surface tension well. As a result, a neighboring molecule, 'C', now feels a net attractive force both into the material *and* along its surface (away from 'A'). Now, given the oppor-

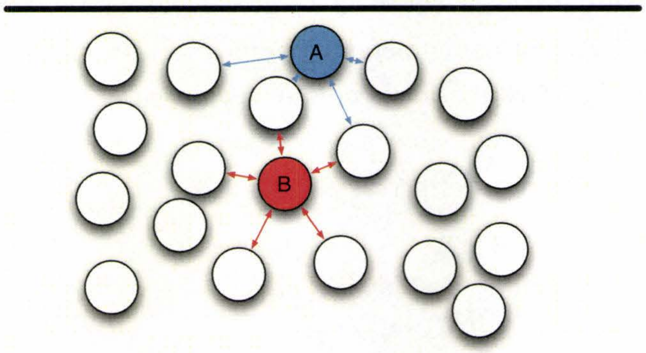

Figure 1.8: A depiction of surface tension.

tunity, 'C' will move away from 'A'. The flow of a material due to gradients in surface tension is known as the Marangoni effect.

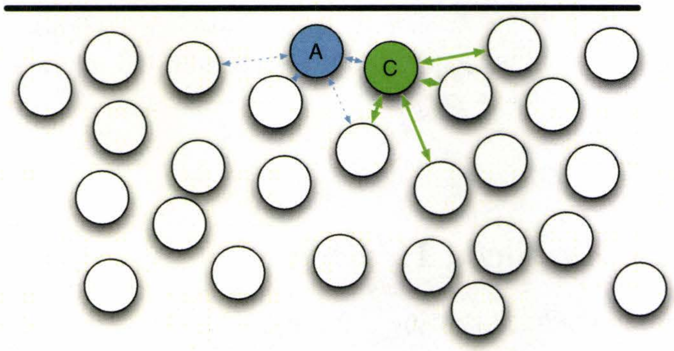

Figure 1.9: A depiction of variations in surface tension.

One way to create surface tension gradients is through local heating of a material. As surface tension depends on the interaction of molecules with their neighbors, and as the strength of these interactions partially depends on the distance between neighbors, it is not surprising that the temperature of the molecules will impact the 'strength' of the surface tension. Due to their higher energy, molecules with a high temperature will tend to be spaced further apart then molecules at a cool temperature. Thus, surface tension is typically inversely proportional to temperature, and a local temperature increase will result in a local surface tension decrease. As shown in figure 1.10, this surface tension gradient will result in a net force on surface molecules directed *away* from the local temperature increase.

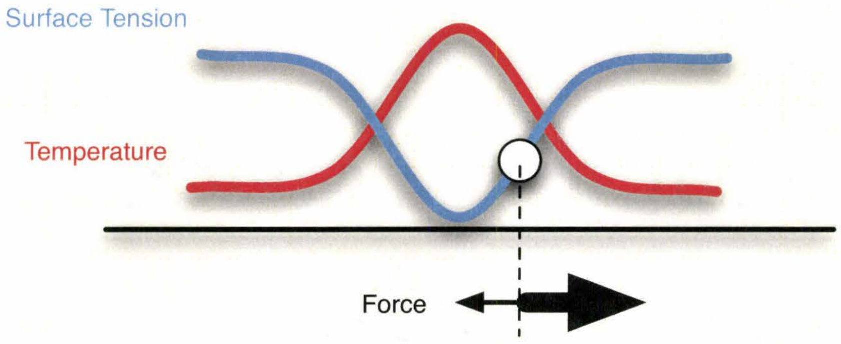

Figure 1.10: Marangoni forces on surface molecules. The surface tension gradient results in a net force pulling a surface molecule (indicated by the circle) away from a higher temperature region.

1.3.2 Laser Induced Heating

The exact method of local heating is unimportant, though to apply the Marangoni effect in a controlled way to create patterns, it should have the following characteristics:

1. In order to allow unencumbered flow, the source of heat should not touch the surface.
2. The intensity and location of the source should be controllable.
3. The size of the source should be comparable to the desired feature size.

A source of heat that adequately meets all of these requirements is a laser beam. A laser beam can heat a surface through absorption of light, meaning that no physical object is in contact with the material that is to flow. Further, its power can typically be adjusted either internally or via external optics. Finally, a laser beam can be focussed to a spot size that is only a few microns wide, enabling the creation of small patterns.

The actual heating effect from the laser is caused by absorption of light by the sample being heated. A typical sample used in laser lithography is a silicon substrate coated with a thin polymer film. As transmission though such a sample is negligible, any light incident upon it is either reflected or absorbed. At normal incidence, the reflectance (or, the fraction of reflected light) of a polymer film with refractive index n_1 on a substrate with a refractive index n_s, is given by the following relationship [16], where n_0 is the refractive index of air:

$$R = \frac{n_1^2(n_0 - n_S)^2 cos^2\delta + (n_0 n_s - n_1^2)^2 sin^2\delta}{n_1^2(n_0 + n_S)^2 cos^2\delta + (n_0 n_s + n_1^2)^2 sin^2\delta}. \tag{1.10}$$

Of note is that the reflectance is dependent on a phase difference, δ, which is defined in terms of the wavelength of light being used, λ, the index of refraction of the film, n_1, and the thickness of the film, t, as [16]:

$$\delta = \frac{2\pi}{\lambda}(n_1 t). \tag{1.11}$$

Values of the refractive indices for materials used in this study are found in Table 1.1. Plotting equation 1.10 with these values, the reflectance of the sample as a function of the film thickness is seen in figure 1.11.

Table 1.1: Optical Properties of Relevant Materials

Material	Index of Refraction (n)
Silicon	4.15 [17]
Polystyrene	1.59 [18]
Poly(methyl methacrylate)	1.49 [18]
P(S-b-MMA)	1.54 [2]

---

[2] As the difference in refractive index between poly(styrene) and poly(methyl methacrylate) is small, and as their phase separated domains are small relative to the wavelength

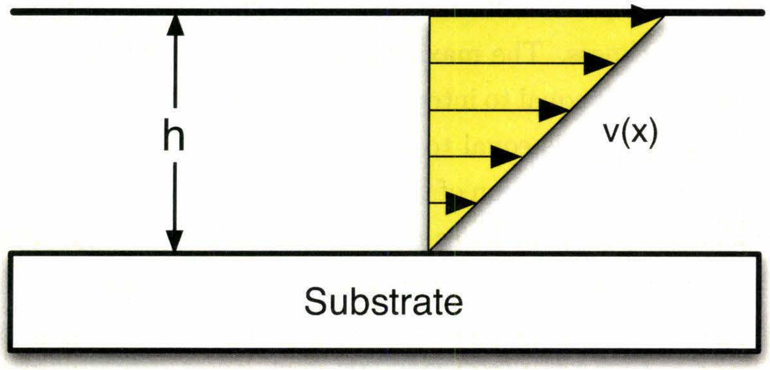

Figure 1.12: Velocity profile in a sheared Newtonian fluid.

This velocity is consistent with what is observed experimentally, in that it is fast enough to account for pattern formation.

The result of a material flow away from a laser heated region is schematically depicted in figure 1.13. Fluid is pulled away from a central region into 'rims' on either side of this heated area. If the laser were left stationary on the film, a 'crater' feature would be formed, while if the laser was scanned across the sample, a 'trench' would be the result. Figure 1.14 is an actual atomic force micrograph depicting both of the cases, well illustrating typical pattern formation via laser lithography of thin polymer films.

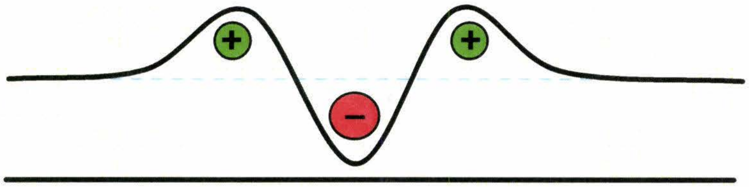

Figure 1.13: Material flow in a locally heated film. Material flows away from the central (heated) region, indicated by the red circle, into two rims, indicated by the green circles. The result is that an originally flat film (dotted line) will develop a 'crater' or 'trench' feature.

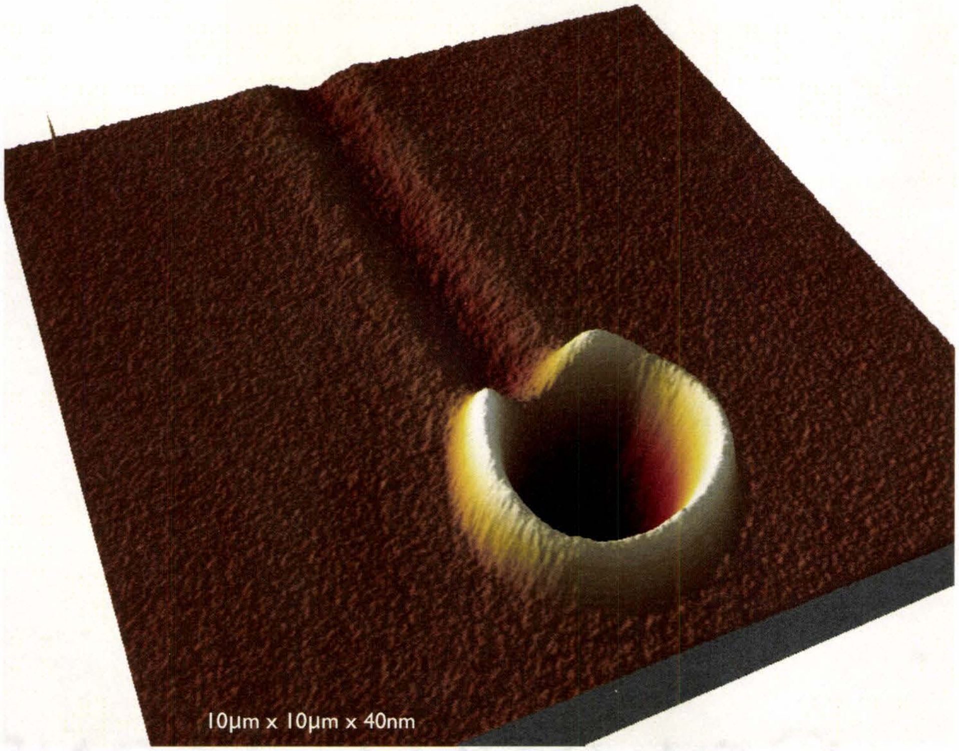

Figure 1.14: AFM image of a patterned 'trench' and 'crater'. This pattern was created by heating a fixed location on the sample for an extended time, resulting in the crater. After this, the laser was scanned across the sample, moving the heated region and forming the trench.

Chapter 2

Experimental Details

Though conceptually simple, the laser lithography experiment still requires a significant number of processing steps. This section discusses preparation of the polymer samples, the actual laser processing of these samples, and how the samples are characterized after the lithography is complete.

2.1 Sample Preparation

The laser lithography experiments done in the course of this research have all used thin polymer films supported by a silicon substrate. Though two methods (spin and flow coating) were used to produce the films, in both cases the preparation of polymeric solutions and the silicon substrates follow the same procedure.

The substrate material is (100) boron doped p-type silicon with a nominal thickness of 500 to 550 μm. The total thickness variation across each of the 100 mm diameter wafers is less then 5 μm, and they are polished on one side only. Prior to substrate coating, the wafer is cleaved into squares with a side length of 9 mm. Though the substrates are blown clean using a compressed gas, no steps are typically taken to remove the native oxide layer of the silicon.

The polymer used in these experiments was obtained from Polymer Source Inc. The main polymer under investigation was symmetric poly(styrene-b-methyl methacrylate) with a number average molecular weight of 18.0 kg/mol per block and a polydispersity index of 1.07 (sample number P2449-SMMA)[21]. Solutions are produced by using a balance to measure out precise quantities of the polymer and of a given solvent. The solvent most commonly used was toluene, purchased from Fisher Scientific (Product Number T291-4). Typical solution concentrations ranged from 0.5% to 5% polymer in solvent, depending on the required thickness. Finally, all solutions were allowed to mix on a Barnstead Lab-Line® MaxQ 2000 shaker for at least 18 hours before use.

2.1.1 Spin Casting

Perhaps the best way to produce the thin, uniform, polymer films needed for the laser lithography experiments is spin casting. Spin casting is a technique wherein a given substrate is flooded with a solution of a polymer immediately before it is rotated at a very high speed. Typically, the majority of the solution immediately flies off of the substrate before the remaining fluid thins out due to the centrifugal force acting on it. The viscosity of the solution increases as the solvent evaporates, until a final steady state thickness is achieved. Films produced in such a way conform to the surface quite well, and are very uniform. Most characterizations of this process have been empirical in nature, and it is accepted that for both newtonian [22] and non-newtonian fluids [23, 24], the final film thickness is strongly dependent on the viscosity of the solution and the spin speed. The initial profile of the solution on the substrate has a negligible effect on the final film thickness, and so can be mostly ignored when producing films in this way.

To create the thin films used in these experiments, a Speedline Technologies® P-6204 tabletop spin coater was used. Prior to coating a substrate, it would be cleaned with compressed air and washed with solvents. One or two drops of filtered polymer solution would be placed on the substrate before spinning. A typical spin profile consisted of the maximum possible acceleration up to a speed that could range from 1500 to 7000 RPM. After keeping a constant rotational velocity for 30 seconds, the maximum deceleration was used to stop the stage. After the spin cycle was completed, the sample would be allowed to "air dry" for several seconds to allow any residual solvent to evaporate.

2.1.2 Flow Coating

An alternative way to create thin polymer films is via flow coating. Since a flow coater did not exist in our laboratory, one was built as part of this M.A.Sc. As it is used in this context, flow coating refers to the applying of a thin layer of polymer solution to the surface of a substrate. As the solvent evaporates, a thin polymer film is left behind. Reviews of this technique by Ruschak [25] and Weinstein [26] show this to be a particularly useful and versatile method of coating large area substrates. Though most treatments of this technique assume Newtonian fluid flow, discussion of non-Newtonian behavior can also be found [27].

Our implementation of this technique is illustrated in figure 2.1. It involves drawing a reservoir of polymer solution across a substrate, leaving a thin layer of solution behind. The solvent in this layer evaporates, leaving a thin film behind. The actual method used to draw the solution across the sample can vary, but typically involves fixing a thin capillary tube just above the sample. A drop of solution is placed onto the tube, creating a reservoir from which the fluid will flow. The substrate is then moved relative to the tube, causing the desired fluid flow.

As described by Ruschak [25], the method that we use to coat the substrate is a "self metering" one, wherein the geometry of the system is kept fixed, and the final thickness depends on the flow properties of the fluid and the speed at which the substrate is moved. Because of the dependance of film thickness on the speed of motion, it is possible to create films with varying thickness by accelerating or decelerating the capillary tube. This technique is a common one used to create thickness gradients in polymer films [28], and is especially useful in the case of diblock copolymer systems [29, 30]. As the pattern formation discussed in this thesis is strongly dependent on film thickness, the flow coating of "wedge" films has proven to be an especially valuable technique.

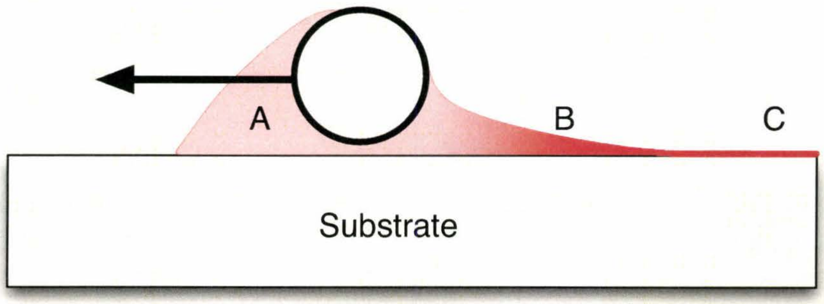

Figure 2.1: The flow coating process. A moving pipette drags a reservoir of solution (A) along a substrate. A layer of the solution (B) is left behind, which slowly evaporates. When all of the solvent has evaporated, a thin film of polymer (C) remains.

Hardware Implementation

Motion control of the flow coater stage is provided by a Newport® LTA-HS Motorized Actuator (High Speed Version) attached to a Newport® 443 Series Linear Stage. Since there is only one axis of travel needed for the flow coater, the actuator is controlled by a Newport® SMC100 Single-Axis Motor Controller/Driver. Mounted on the 443 stage is a Thorlabs® KB3X3 Kinematic Base, to which an Omegalux® SFRG-202/5 Flexible Silicone Rubber Fiberglass Insulated Heater is attached. This heater allows for heating of the substrate during flow coating, which enhances the evaporation rate of the solvent and allows for the coating of polymers that remain in solution only at high temperatures.

The substrate to be coated is typically 'glued' to a microscope slide with a low concentration polymer solution. The slide is then mounted onto the KB3X3 Base, after which a Kimble® melting point capillary tube is balanced onto the sample. The tube itself is then glued to a set of fixed posts on either side of the stage, keeping it from rotating during flow coating. Finally, a drop of polymer solution is placed on the substrate at the location of the tube, after which the stage is commanded to move with the desired velocity profile.

Software Implementation

The SMC100 Motor Controller is itself controlled by a computer running a custom LABVIEW-based application. This software allows for initialization of the controller, positioning of the sample, simplifies the creation of velocity profiles, and reports on the status of the system. Each of these aspects is described in more detail below:

Initialization - On startup, the software initializes a Virtual Instrument Software Architecture (VISA) session with the controller. Along with this, the controller and actuator are 'homed', and a maximum travel distance of 40 mm is imposed. The travel limit is intended to prevent the actuator from reaching its hardware travel limit (50 mm) in case of erroneous user input.

Sample Positioning - In order to most effectively coat the sample, it is necessary to position it relative to the capillary tube such that the tube is located near the edge of the sample. To this end, these are a series of controls which enable fine-grained sample positioning. The software polls all sample positioning controls every 500 milliseconds in order to determine if any user inputs have been made. These inputs can be in one of two forms. First, dragging a slider representing the actuator will cause the software to immediately command a move to the requested position. Alternatively, a specific extension of the actuator can be specified, in which case the software will wait until the 'Go' control is activated before moving. In either case, the software will not permit movement beyond 40 mm.

Sample Coating - When coating the sample, three scan types are possible; including Constant Velocity, Constant Acceleration, and Complex Profile. For each of these, the software will take the user input, check the resulting velocity profile to make sure that no hardware limits are being exceeded, and then command the controller to perform he desired movement. The Constant Velocity setting reads in the size of the substrate and the desired velocity, and accelerates the actuator at a very high rate (20 mm/s^2) up to the selected velocity. The Constant Acceleration setting reads a velocity and calculates the acceleration required to achieve this velocity given the size of the substrate. Finally, the Complex Profile setting allows for the user to specify multiple accelerations. This is done by inputting the distance over which the acceleration is to occur along with the ultimate required velocity. Examples of each of these profiles are given in figure 2.2. Two limitations of the motion controller hardware are of note. First, the controller must come to a stop before a new acceleration is started; and second, acceleration and deceleration values must be equal for any given movement. Though not important for simple applications, these limitations prevent this implementation of a flow coater from creating a two-component wedge, for example.

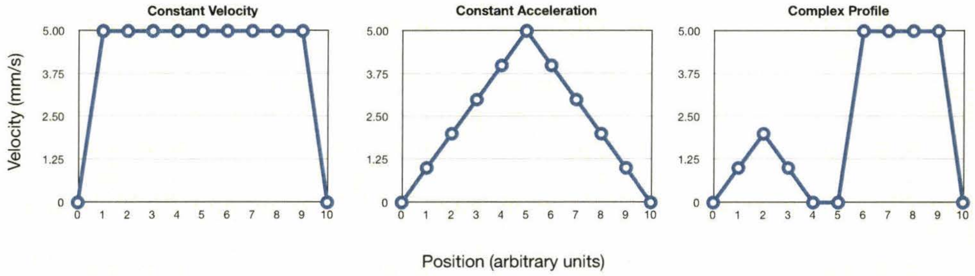

Figure 2.2: Flow coater velocity profiles.

Controller Status - The controller status routine polls the controller and displays its status. The controller can be in one of the following states: Not Referenced, Configuration Mode, Homing, Moving, Ready, Disabled or Jogging. These states are used both by the software and by the user to control the timing of events.

2.2 Sample Processing

Once a thin polymer film has been prepared by one of the above mentioned methods, it can undergo laser lithography. The experimental setup consists of an optical system controlled via a custom LABVIEW-based application. This section is a description of both the hardware (optical and otherwise) and the software used in the implementation of this experiment.

2.2.1 Optical Systems

Though the laser lithography apparatus is in principle quite straightforward, a significant number of optical and opto-mechanical components are required in order to produce the required laser spot characteristics at the surface of the sample. Broadly, the apparatus can be divided into two sections. The first section, as illustrated in figure 2.3, generates the laser beam and controls the total power delivered to the sample. It includes the laser itself, a half wave plate, a polarizing beam splitter, a beam stop, a shutter and an optical chopper. The second section, as illustrated in figure 2.5, focusses the laser beam onto the sample. Included in this section are several mirrors, a 10x focussing objective, an optical power meter and the temperature- and motion-controlled stage that the sample is mounted on. The following will be an item-by-item discussion of each component in this optical system, as labelled in figures 2.3 and 2.5.

Component A - Laser

The laser beam itself is generated by a Coherent® Verdi™ V-2 continuous wave solid state laser. This is a frequency-doubled neodymium-doped yttrium aluminum garnet (Nd:YAG) laser that outputs green light at 532 nm[31]. The beam at the exit aperture of the laser has a diameter of 2.25 mm ± 10%, and is polarized vertically with respect to the surface of the optical table. The polarization ratio of the laser is 100:1 (vertical to horizontal polarization). Detailed specifications of the laser are found in Appendix A [32]. The laser is connected to a computer via a GPIB interface, allowing for remote, preprogrammed laser power control.

Component B - Half Wave Plate

As output from the laser, the beam is linearly polarized in the vertical direction

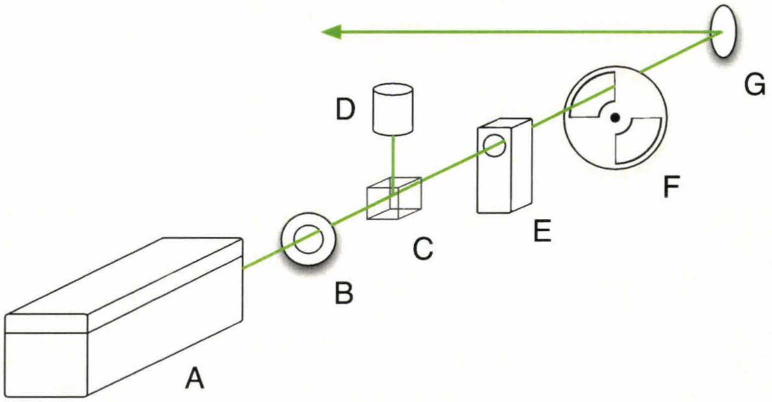

Figure 2.3: Optical system - Section A. This section includes the laser (A), a half wave plate (B), a polarizing beam splitter (C), a beam stop (D), an external shutter (E), an optical chopper (F), and several mirrors (represented by G).

with respect to the surface of the optical table. The half wave plate serves to rotate the polarization of the light to any arbitrary angle. A Newport® 05RP02-16 Zero-Order Waveplate is mounted on a Newport® MT-RS Compact Rotation Stage, allowing for its manual rotation. This component works in conjunction with the Polarizing Beam Splitter to allow for much finer control of the laser power reaching the sample, as described below.

Component C - Polarizing Beam Splitter

The beamsplitter used in the laser lithography apparatus is a Newport® 05BC16PC.3 Polarizing Cube Beamsplitter. This beamsplitter separates incoming light into two linearly polarized orthogonal components. The p-polarized (vertically polarized) component of the light is transmitted, while the s-polarized (horizontally polarized) component is reflected, with an extinction ratio of 1000:1 [33].

If the unmodified beam from the laser (which produces vertically polarized light) were incident on the beamsplitter, almost 100% of the light would be transmitted. The amount of transmitted light is changed by modifying the polarization of the incoming light, which is accomplished by Component B —

the half wave plate. This rotates the vertically polarized beam, resulting in linearly polarized light that has both vertical and horizontal components. Any horizontal polarization is reflected out of the beam by the beamsplitter, reducing the total intensity. As shown in figure 2.4, this can be used to attenuate the light over a very broad range.

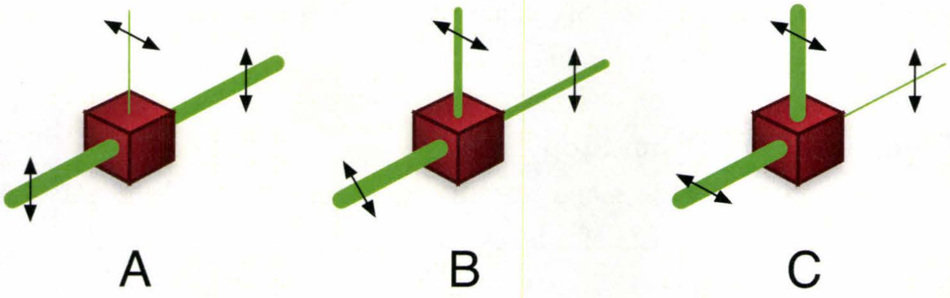

Figure 2.4: Function of the polarizing beamsplitter. The arrows indicate the polarization of the corresponding light, while the thicknesses of the green lines represent the relative intensity. In case A, the incoming light is vertically polarized, resulting in the majority of light passing through the beamsplitter. In case B, the incoming light is polarized at 45° with respect to vertical polarization, with the result that half the light passes though the beamsplitter and half is rejected. In case C, the incoming light is horizontally polarized. The result is that almost all of the light is rejected.

This technique can also extend the range of laser powers available, as well as the resolution at which we can select laser powers. Firstly, by attenuating the beam, the use of laser intensities that are much lower then the lowest laser output powers are possible. These lower incident powers can be achieved while maintaining moderate-to-high laser output powers, allowing the laser to operate in its most stable regime. Additionally, by reducing the total incident power in this way, we increase the resolution of the laser at the expense of maximum available incident intensity. For example, if the beamsplitter is used to attenuate the output beam by 50%, a change to the absolute laser output power of δ will only change the incident power by $\delta/2$, effectively doubling the power resolution at the cost of reducing maximum incident power to half of the total output power.

Though other techniques (for example, neutral density filters) can be used to attenuate the beam, the beamsplitter approach has several advantages. First, since a minimal amount of light is absorbed by the optical components, this technique is suitable for higher laser powers. Further, since attenuation is dependent of the degree to which the incoming light is horizontally polarized, and since this can be smoothly adjusted via the waveplate, attenuation is not limited to specific discrete values.

Component D - Beam Stop

The Beam Stop captures and absorbs the light rejected by the Polarizing Beam Splitter. It consists of a black 90° section of $\frac{15}{16}$-inch copper piping and is designed to minimize the scattering of light in the laser laboratory. As the laser beam is defocused at this point in the optical system, damage caused by extremely high local temperatures is not a significant risk. Thermal heating of the beam stop assembly is typically quite mild, even at relatively high laser powers.

Component E - External Shutter

Though the laser is equipped with a shutter (hereafter referred to as the "internal shutter"), it is desirable to have a second independent shutter early in the optical system. This "external shutter" allows for very precise control of sample illumination when it is needed for timed experiments. It also enables pre-illumination power adjustment (using the waveplate / beamsplitter arrangement) and laser stabilization. The specific shutter used is a Newport® 846HP Electronic Shutter, which can safely control laser illumination at all currently available laser powers. Additionally, its 10 ms response time enables very accurate timing experiments [34]. The shutter is connected to a National Instruments® PCI-6035E DAQ via an SCB-68 Connector Block, allowing for software control of shutter triggering.

Component F - Optical Chopper

In addition to the external shutter, it was found necessary to include a way to regularly and suddenly cut off sample illumination independently of the control software. A Thorlabs® Model MC1000 optical chopper was used for this purpose. A 2-slot blade enables chopping frequencies between 1 and 99 Hz.

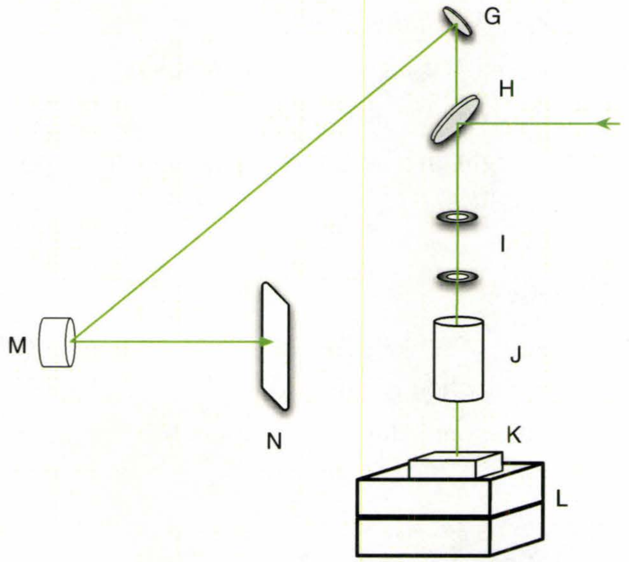

Figure 2.5: Optical system - Section B. This section includes several mirrors (G), a laser mirror (H), two irises (I), a 10x objective (J), a heating stage (K), an actuator stack (L), an optical power meter (M), and a viewing screen (N).

Component G - Periscope and Mirrors

By far the most numerous components in the second section of the lithography apparatus are the broadband mirrors. These mirrors are typically Newport® 10D20BD.1 Broadband Dielectric Mirrors, which reflect over 99% of light at 532 nm. They are used to guide the beam from the last component of the first section (the optical chopper) to the first component of the second (the laser mirror). The mirrors are also used to increase the optical path length between the laser mirror and the viewing screen, which allows for more precise focussing of the laser onto the sample.

Component H - Laser Mirror

This first component of the second section of the optical setup is a CVI Laser Corporation® Y2-1025-45-UNP Nd:YAG Laser Mirror. The purpose of this mirror is twofold. First, it reflects the laser beam down through the irises and into the objective. Secondly, it allows some of the light that has reached the sample and reflected back up through the objective to reach the viewing screen. The mirror is able to accomplish this because it is not completely reflective for 532 nm light at the angle is is being used (approximately 45°), allowing enough light through to be used for focussing purposes.

Component I - Irises

Two irises in line with the objective are used for alignment purposes. The laser is correctly aligned when it shines though the center of both irises. Under normal operating conditions, the irises are left fully open and do not interact with the beam in any way.

Component J - Objective

The purpose of the objective is to focus the laser beam to a spot size that will generate the necessary thermal gradients in the polymer film. A Mitutoyo® M Plan NIR 10x objective is used to accomplish this focussing. This objective has a focal length of 20.0 mm, and given the beam divergence of the laser, the minimum focal spot size can be calculated [16]. This calculation is done in Appendix B, with the result being a minimum spot size of 6.00 μm.

Component K - Heating Stage

It is necessary to control the background substrate temperature both before and during laser lithography. This is normally done to have the polymer film near or above its melting temperature. A molten polymer film can be treated much more simply then a polymer film which is glassy, though interesting behavior can arise when the only molten region is that which is being actively heated by the laser.

A Linkham® THMS 600 heating stage connected to a TP 94 temperature controller provides this capability. The temperature controller is connected to the computer via an RS-232 cable, and so can be adjusted either manually or using the laser lithography software.

Component L - Actuator Stack

In order to create extended features, it is necessary to move the sample in a controlled way during the laser lithography process. Two Newport® 423 Series High-Performance Low-Profile Ball Bearing Linear Stages are mounted orthogonally to each other and are actuated with a pair of Newport® CMA 25CCCL Compact Motorized Actuators. The actuators are connected to a Newport® ESP 300 Motion Controller/Driver. These provide x- and y- axis motion control, enabling the creation of any arbitrary two dimensional patterns in the polymer films. As it is essential that the motion of the stage be coordinated with the laser output power and each of the two shutters, the ESP 300 is connected to the computer via a GPIB interface and is controlled with the laser lithography software.

Component M - Detector

The most direct way to monitor the absorbed power for a given laser output level is to measure the amount of light that is reflected from the sample. The laser mirror (component H) allows some reflected light to pass through itself, which is redirected by a series of mirrors to a detector. Though not all of the reflected light is collected, changes in the power arriving at the detector are directly related to the total power reflected, and so can be used to monitor absorbed power.

The detector used is a Newport® 818-SL Low Power Detector connected to a Newport® 1830-C Optical Power Meter via a calibration module. Since it is necessary to monitor the power as the laser lithography proceeds, the Optical Power Meter is connected to the GPIB bus, and in turn, monitored by the laser lithography software.

Component N - Viewing Screen
Light that is reflected from a sample is partially transmitted though the dielectric mirror and guided to the viewing screen by the detector and a series of mirrors. The image formed on the screen can be used to monitor the focus of the laser beam onto the sample.

2.2.2 Software Control

As mentioned, the laser lithography process requires extensive coordination between the motion control stages, the shutters, and the laser power. The most reasonable way to do this was by controlling these key aspects of the experiment via a computer. A LABVIEW$_{®}$ application was developed specifically for this task. The program has undergone several revisions, and has become an extremely flexible tool in creating arbitrary patterns using the laser. A basic overview of the program is given in figure 2.6.

Immediately upon being run, the program initializes basic settings of the laser lithography system. As long as the program is not terminated and not commanded to begin creating a pattern, it continuously polls the control panel and makes any requested changes. When a scan is initiated, the program coordinates the motor stages and laser to create the requested pattern. The parameters for any given pattern are stored as a tab-delimited text file. Each of these steps is outlined more fully below.

Initialization The program first initializes all of the connected equipment in order to prepare it for the coming series of commands. This involves turning the motors on and executing a “search for home” routine using an initial set of motion parameters (velocity, acceleration and deceleration). The axes are then grouped together so as to allow simultaneous motion. Finally, communication with the other pieces of equipment is initialized.

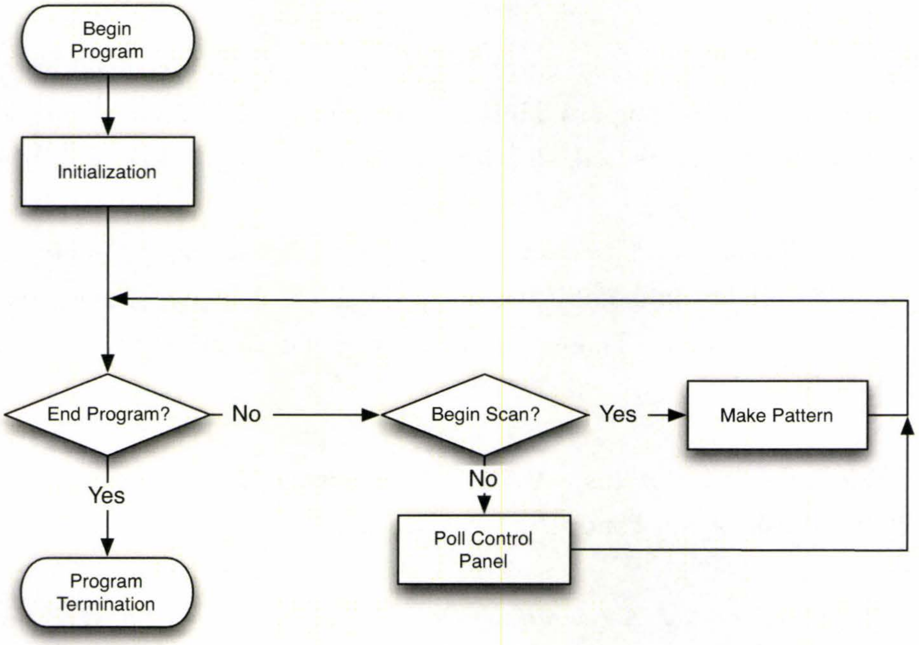
Begin Program
Initialization
End Program?
No
Yes
Program Termination
Begin Scan?
Yes
No
Make Pattern
Poll Control Panel

Figure 2.6: Flow diagram of the controlling LABVIEW program.

Control Panel Polling As long as the program is not terminated or pattern formation has not been initiated, the program polls the control panel every 25 milliseconds for user input. If user input is detected (by observing a change in a control parameter), appropriate action is taken by the program to accommodate the changed settings. The following parameters are monitored:

Temperature Setpoint - If this is changed, the program sends appropriate commands to the temperature controller to adjust the setpoint temperature.

Selected Pattern - If the currently selected pattern is changed, the corresponding file is read and parsed into a multidimensional array. From this array, a scan simulation is created, showing the expected path of the laser beam.

Power Setpoint, Main Shutter Status - A change in this parameter results in an appropriate command being set to the laser, changing either power output or shutter status. These can be adjusted independently (i.e. the power can be adjusted even with the main shutter closed).

External Shutter Status - A command is set to the external shutter to reflect the status of this control.

Vectorial Velocity, Acceleration, Deceleration - These parameters are controlled by the motion controller, so a change in any of them result in an appropriate command being sent to the ESP 300.

Timeout - If no parameters have been changed since the last control panel polling, the "timeout" routine is activated, which preforms various housekeeping tasks. Most notably, the temperature of the stage is measured and displayed.

Drawing a Given Pattern If the "Begin Scan" control is activated, the program ceases to poll the front panel controls and begins to draw the appropriate pattern using the laser. The pattern is taken from an input file, which contains all of the instructions needed. The file is a tab-delimited text file, where each line in the file represents a 'feature' to be drawn. Each line contains seven separate fields, as follows:

1. Feature Number - Identifies the feature. This is for the reference of the user, and not used by the software.

2. Feature Type - Selects the type of feature. A '0' here will draw a dot, a '1' is a line-starting waypoint, a '2' is a line-continuing waypoint, and a '3' is a line-ending waypoint. These last three features allow for the drawing of multi-component lines. For example, a straight line consists of two features (a start ('1') and an end ('3')), while a 'vee' shape consists of three features (a start, a midpoint ('2') and an end).

3/4. x- and y- Coordinates - The spatial coordinates of the feature.

5. Velocity - The velocity that will be used to move to the feature.

6. Delay - The number of milliseconds the external shutter will remain open after the feature is complete. This is typically used to control the exposure time of the 'dot' features.

7. Power - The laser power requested for the current feature.

This type of parameter file format allows for very flexible pattern definitions, and allows the rapid reproduction of any given pattern. Examples of the varied patterns that are possible are given in figure 2.7

Once the input file is read into an array, the program begins at the first feature and 'draws' the entire pattern. Of note, however, is that before each feature is drawn, the program corrects for backlash in each of the actuators. The logic used to correct the backlash is outlined in Appendix C.

2.3 Sample Characterization

The samples created using laser lithography were characterized by optical and atomic force microscopy. This section briefly describes how these techniques work and the parameters they were used to measure.

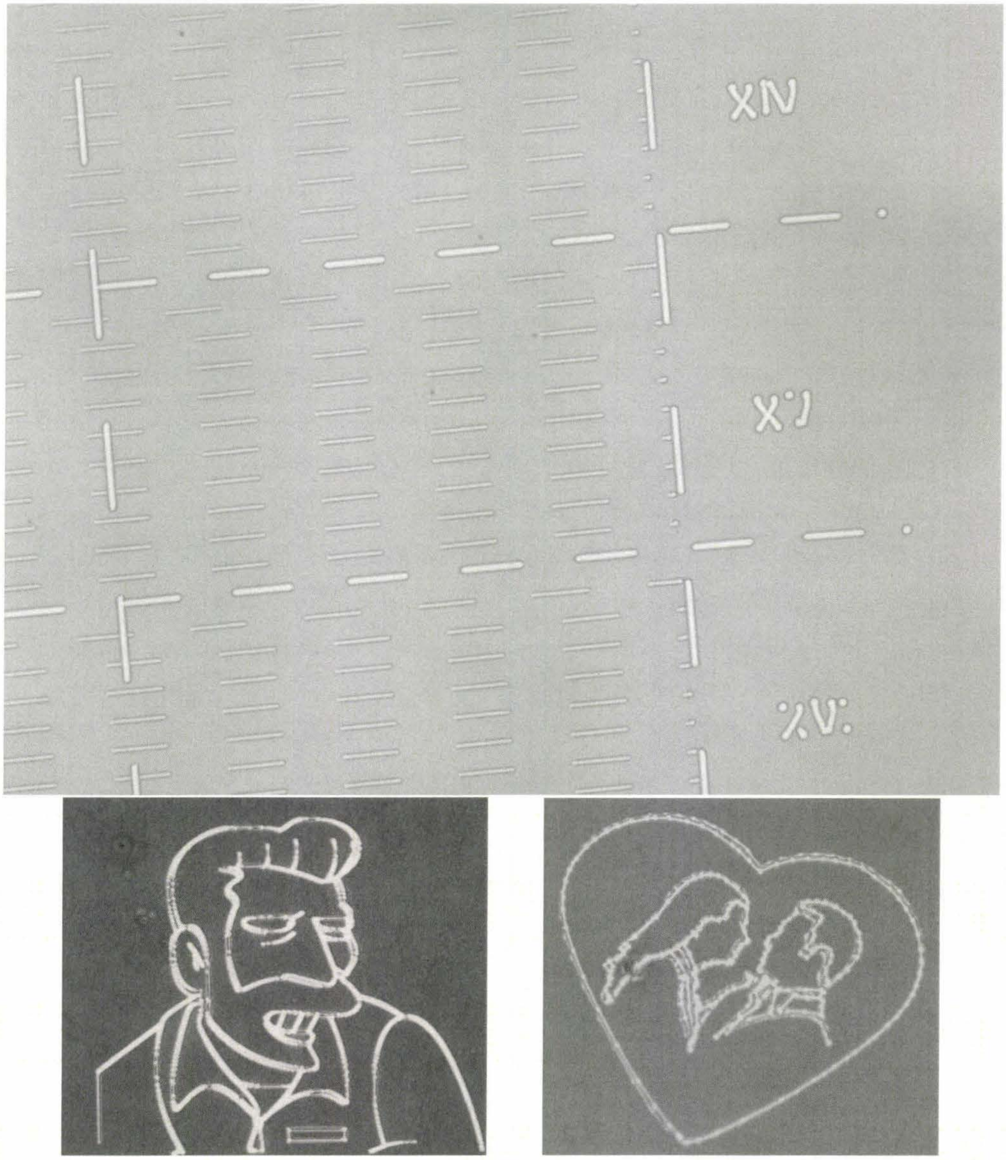

Figure 2.7: Examples of various patterns. The laser lithography software enables the creation of varied patterns in thin polymers films. The top image is an example of the type of pattern used to explore the 'parameter space' of the system. The bottom two images illustrate the flexibility of the system in creating any arbitrary 2-dimensional pattern. Thanks to Joshua McGraw for the artwork on which the 'wedding' image is based.

2.3.1 Optical Microscopy

Optical microscopy has a long and distinguished history, with modern microscopes being able to produce diffraction-limited images of many types of samples. The microscope used in these experiments was an Olympus® BX51 Research Microscope. Mounted on the microscope were Olympus® UMPlanFl 5x, 10x, 20x, 50x and 100x objectives. Images were captured with a Photometrics® CoolSNAP FX camera and the Media Cybernetics® Image Pro Plus 6.1 software package.

Optical microscopy has the advantage of rapid image acquisition, and so was used heavily during the sample processing stages to ensure that the desired patterns were being created. Further, it was used to identify interesting areas of the sample that were to be examined more carefully on the atomic force microscope.

One of the parameters of interest in characterizing the samples was the spacing between patterned features. Optical microscopy was used here to capture images of the patterns that were subsequently analyzed to obtain these spacings. Of note is that many of the patterns of interest had lateral dimensions that were on the order of microns. To obtain sufficient magnification to observe the patterns, the 100x objective needed to be used. In order to ease analysis, the resulting captured images were processed using Image Pro Plus to enhance their contrast. Figure 2.8 demonstrates the results of such processing.

Though the limited resolution of optical microscopy would seem to indicate that sub-micron sized features are not measurable, this is not the case. For example, for thin polymer films on silicon, interference effects are very important. The strong thickness-dependent changes in reflectivity due to interference allow the measurement of nanometer-scale changes in the hight of the film. As shown in figure 2.9, this is especially the case in organized copolymer systems, as these can exhibit sharp thickness variations.

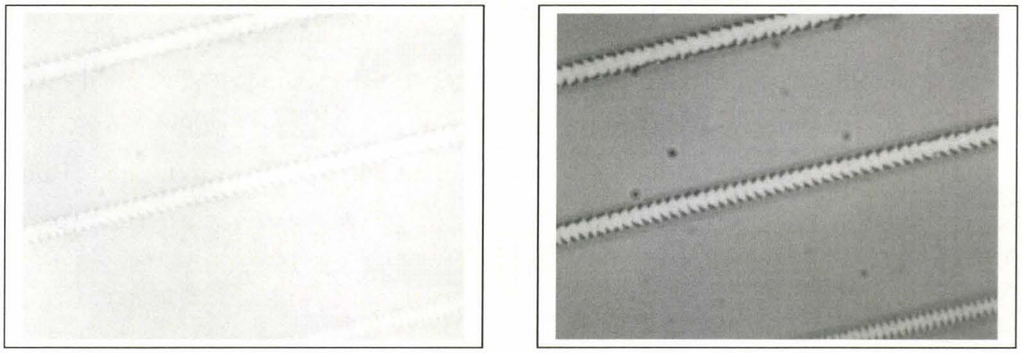

Figure 2.8: Results of contrast adjustment. The image on the left is unprocessed, while that on the right has has its brightness, contrast and gamma adjusted in order to ease analysis.

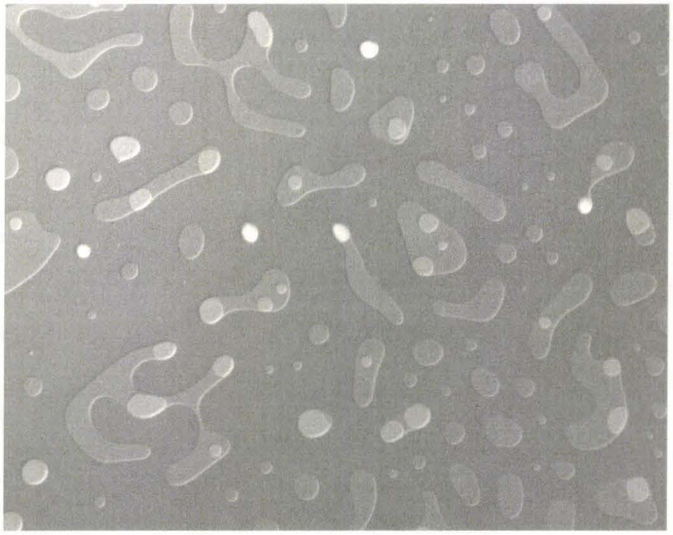

Figure 2.9: Optically measurable thickness variations. This sample consists of a series of holes and islands in a diblock copolymer film. The change in thickness from one layer to the next is ~20 nm.

2.3.2 Atomic Force Microscopy

One limitation of optical microscopy is the resolution it provides, especially when using a visible light source. An alternative method of viewing the samples is via an Atomic Force Microscope (AFM). Though much slower then optical microscopy, it provides ultra-high resolution topographic maps of the samples. The AFM is an offshoot of the Scanning Tunneling Microscope (STM), the development of which resulted in a Nobel Prize in Physics for Gerd Binnig and Heinrich Roher [35]. Both of these techniques can be classified as Scanning Probe Microscopy, as they depend on moving (or 'scanning') a very fine probe across a sample. In the case of STM, a very fine probe is brought near to the surface of a sample, remaining separated from it by a small vacuum gap. After applying a potential difference between the probe and the sample, information regarding sample topology and composition can be obtained by measuring the magnitude of the current tunneling through the gap [36].

As opposed to using tunneling current, an atomic force microscope can obtain topographic information by quite literally 'feeling' the surface of the sample. As illustrated in figure 2.10, an atomic force microscope consists of a long cantilever tipped by a sharp probe. The cantilever can be precisely positioned relative to the surface of the sample using piezoelectric actuators. A laser beam is reflected from the top of the cantilever to a spilt photodiode, which enables the deflection of the cantilever to be measured. In *contact mode* imaging, the probe is brought into direct contact with the sample. As the probe is scanned across the surface, any topographic features will cause a deflection of the cantilever. This deflection is measured with the split photodiode, and a topographic map of the surface is created. In *non-contact*, or *tapping mode*, imaging the cantilever is oscillated just above the surface of the sample at a frequency very close to its natural resonance. As the tip of the probe is brought closer to the sample, the interaction between the sample and the surface will cause a change in the amplitude of the oscillation. By monitoring this amplitude and adjusting the height of the probe to keep it constant, the tip of the probe can be kept at a fixed distance from the surface without having it in continuous physical contact. As the magnitude of the physical interaction between the tip and the surface is only significant at the 'bottom' of the oscillation, tapping mode imaging is much more gentle then contact mode, and is therefore the favored technique when imaging soft samples [37, 38].

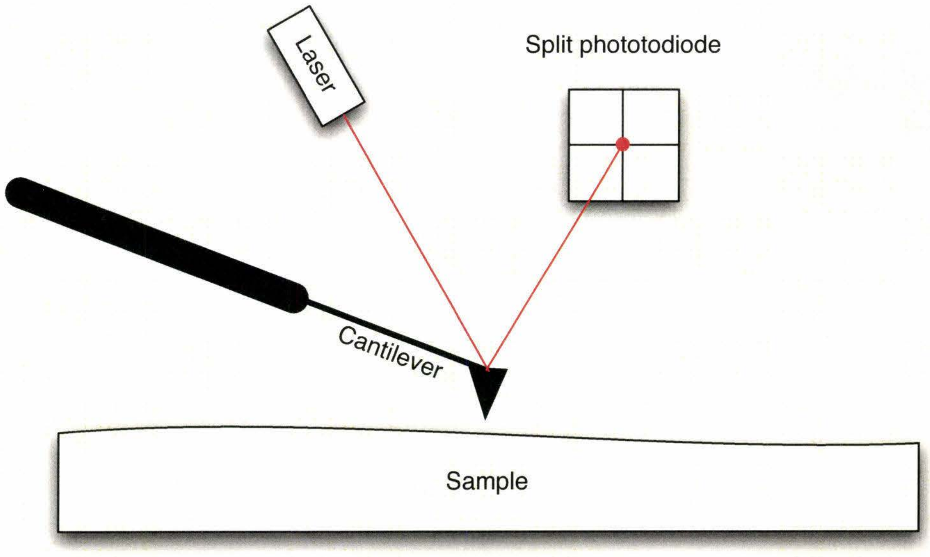

Figure 2.10: Schematic diagram of an atomic force microscope.

The specific instrument used in this experiment was a Veeco® Caliber Scanning Probe Microscope mounted on a Halcyonics® Mod-1 vibration isolation unit. Veeco® SPMLab software was used to capture the images, which were later processed using SPIP™ from Image Metrology®. Due to the sensitivity of polymer films, tapping mode imaging was exclusively used.

Chapter 3

Results and Discussion

Laser lithography of homopolymer films has already been shown to be a novel method of patterning structures ranging from microlens arrays to microfluidic devices [19]. These structures have all been limited by the resolution of the patterning technique to sizes on the order of microns. However, when applied to diblock copolymer films, interesting patterns on the nanoscale can be produced. This section discussed the results of applying laser lithography to symmetric diblock copolymer films. The observed behavior is described, followed by an analysis of the effects of parameter variation on the formation and growth of these patterns.

3.1 Observed Behavior

While the patterns created using diblock films share some of the characteristics of laser lithography as described in section 1.3.3, they are obviously different in several ways. Figure 3.1 is an atomic force micrograph of typical patterns created via laser lithography of thin homopolymer and diblock copolymer films. The familiar 'trench' and 'crater' features are still present in the diblock case, though they are significantly different.

Of the several features that are of particular interest, the most outstanding is the patterning of the 'trench'. Whereas laser lithography of a homopolymer film resulted in a smooth trench with continuous 'rims' on either side, the

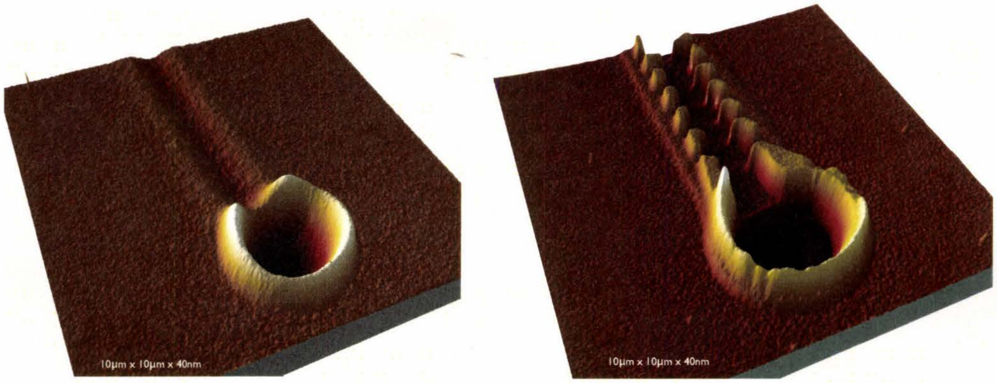

Figure 3.1: A comparison between laser lithography of homopolymer films (left) and diblock copolymer films (right).

diblock sample shows a very distinctive series of 'islands' atop a continuous raised ridge. Furthermore, where the homopolymer sample shows a smooth and continuous 'crater' feature, the diblock sample shows a 'crater' whose rims are flat in places and nearly pointed in others.

Further experimentation discovered related patterns that could be created using the diblock films. Figure 3.2 shows a trench that consists of a series of evenly spaces holes bracketed by two lines of evenly spaces islands. These patterns are remarkable in the range of length scales that they exhibit. Typical patterns are only about 40 nm 'tall', approximately 3 μm wide, and display the same regularity over macroscopic lengths of centimeters.

When an optical chopper was used to abruptly cut the incident laser power to the samples, a view of the 'ends' of the trench can be seen. This allows for the taking of a 'snapshot' of the pattern as it is being formed. Figure 3.3 gives a view of two ends of a trench. The first end occurs when the laser is suddenly shone onto a moving sample. We see here the initial stages of pattern formation. The second 'end' shown occurs when the laser power is abruptly cut while pattern formation is occurring.

It is obvious that, although the typical Marangoni induced flow is still present, there are other contributions that result in the generation of these unique features. It was hypothesized at an early stage of this work that these

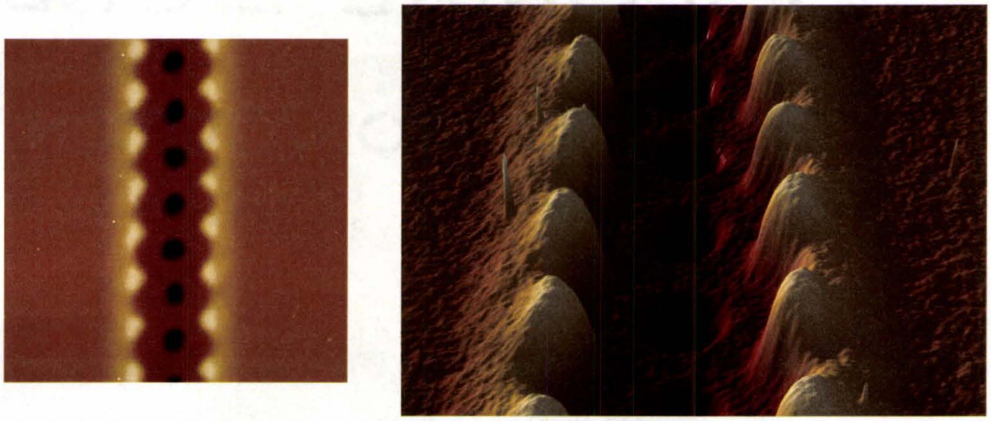

Figure 3.2: Example of patterned diblock copolymer films. This P(S-b-MMA) film has been patterned using laser lithography. The image on the left is a 10 μm x 10 μm atomic force micrograph, with a vertical (z-axis) range of 66 nm. The image on the right is a 3-dimensional representation of the same data.

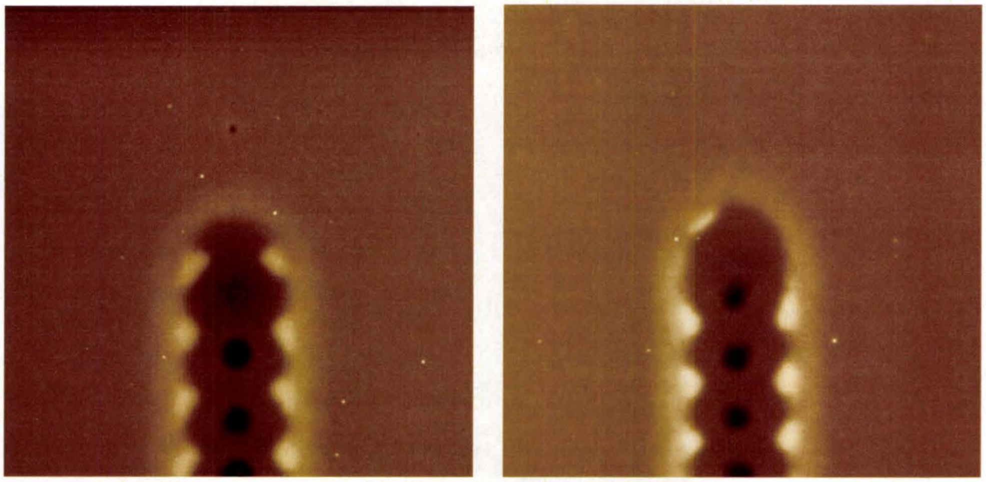

Figure 3.3: A view of pattern 'ends'. The left AFM image shows the initial formation of a pattern, while the right shows the 'end' of the pattern when laser power is abruptly cut. The scan area for each image is 10 μm x 10 μm.

patterns are formed via the complex interplay between the Marangoni flow and the tendency for the diblock molecules to self assemble into lamella. A series of experiments was performed in order to characterize these patterns and gain insight into their origin.

3.2 Effects of Parameter Variation on Patterning

Five main parameters were adjusted in order to determine their impact on pattern formation. They included the composition of the films, the velocity of the laser scan, the output power of the laser, the thickness of the film and temperature at which the laser lithography experiment was conducted. Each of these is discussed below.

In order to characterize the effects of these changes, it was necessary to have a 'yardstick', a quantitative measure of some relevant dimension of the pattern. It was decided to use the period of the pattern in this role. As used in this section, the period of the pattern is defined as the spacing between successive 'islands' on the rims of the trenches. To improve measurement accuracy, an average distance between a number of islands (typically between 10 and 30) was used.

3.2.1 Film Composition

In order to determine whether the interesting diblock pattern formation was actually due to the unique structure of the diblock copolymer molecule, it was necessary to compare various film compositions. As the diblock used was P(S-b-MMA), films of polystyrene and poly(methyl methacrylate) were prepared, along with a film composed of a 50%-50% PS/PMMA blend. The films were all spuncast to approximately the same thickness in order to facilitate comparison. Laser lithography of these films consisted of a series of lines with varying power. Figure 3.4 shows the results of these experiments at relevant laser power levels.

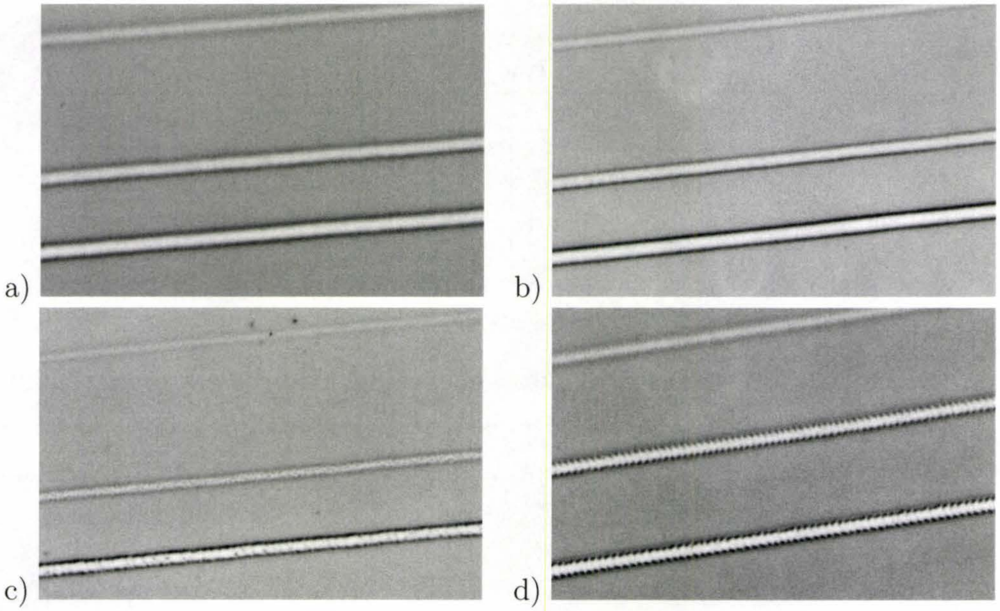

Figure 3.4: Optical micrographs of pattern formation in various polymers: a) PS (homopolymer), b) PMMA (homopolymer), c) PS/PMMA (homopolymer blend), and d) PS-b-PMMA (diblock copolymer). The imaged area in each case is approximately 70 μm x 110 μm.

The polystyrene and poly(methyl methacrylate) homopolymer films show no pattern formation for any of the lines produced. The blend film does exhibit some interesting features, including what appears to be small 'clumps' of polymer within the trenches. These can be attributed to phase separation of the two film components that occurred during the time that the film was heated by the laser. It is of note that these is no apparent regularity to the phase separated areas. The diblock copolymer film, as previously discussed, does show the characteristic regular pattern. Table 3.1 summarizes these results.

Table 3.1: Pattern Formation in Various Polymers

Polymer	Molecular Weight	Pattern
Poly(styrene)	93.2 kg/mol	No
Poly(methyl methacrylate)	18 kg/mol	No
50%-50% PS/PMMA blend	15 kg/mol / 18 kg/mol	No
P(S -b- MMA)	(18 -b- 18) kg/mol	Yes

This result is one piece of evidence confirming that the patterning is due to the diblock molecule. This test also helps to eliminate other possible sources of the pattern, including mechanical vibration of the stage. A mechanical vibration would tend to induce a pattern in all films, not only in the diblock samples.

3.2.2 Scan Velocity

A second test performed on the diblock patterns was to change the velocity of the stage during laser lithography. Recall that 'trenches' are produced by scanning the sample at a given velocity relative to a stationary laser spot. Changing the speed of this scan gives insight into how the pattern is being produced.

Laser lithography of a diblock sample was performed using a constant laser power of 0.34 W. A series of lines was produced by varying the speed of the laser scan between 60 and 140 μm/sec. The period of the pattern on each of these lines was measured, with the results shown in figure 3.5.

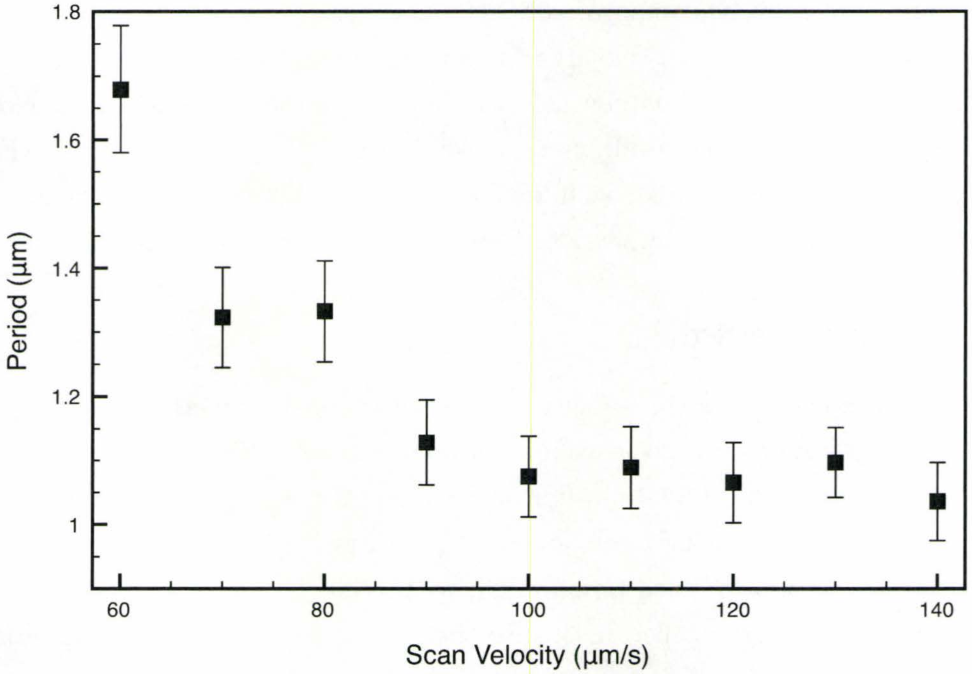

Figure 3.5: Period as a function of scan velocity for a constant laser power output of 0.34 Watts. For this experiment, the half wave plate was set to allow nearly 100% of the laser output through the beamsplitter, enabling the production of patterns at relatively low laser output powers.

Slower scan speeds result in the laser heating a given volume of material along its path for a longer time. As long as the temperature gradient is maintained, material has the opportunity to flow due to the Marangoni effect. It is therefore expected that a slower laser scan would result in larger patterns. This is in fact what is observed. It is interesting, however, that while there is a significant drop in period from 60 to 90 μm/sec, from 90 to 140 μm/sec there appears to be comparatively little change.

The 55% increase in velocity from 90 to 140 μm/sec results in a decrease in period of only approximately 10%. In comparison, the 50% increase in velocity from 60 to 90 μm/sec results in a period decease of approximately 35%. From this, it is reasonable to conclude that although initial pattern formation is relatively rapid, there appears to be some delay before the pattern grows.

3.2.3 Laser Power

Aside from adjusting the velocity of the scan, an obvious method to change the absorbed power for a given volume of material is to adjust the output power of the laser itself. A 34.4 nm film of PS-b-PMMA was prepared, and a series of lines with increasing laser powers were written. Figure 3.6 is a plot of the pattern's period for each power used, with each data point representing the period of a separate line. Inset into the figure are atomic force micrographs showing the pattern corresponding to four distinct lines.

Several features of this plot are immediately obvious. There appear to be two distinct regions of pattern growth, above and below a laser power of approximately 1.22 Watts. For laser powers below this threshold, the pattern grows slowly from a period of 0.8 μm to 1.1 μm. Above 1.22 Watts, the pattern grows at a significantly faster rate, reaching a period of nearly 3 μm for a laser power of approximately 1.25 Watts.

Of note is the morphology of the pattern as the power increases. Pattern growth appears to occur at the slower rate until the islands on either side of the trench are large enough to come into contact with each other. Once the islands touch, they begin to merge together and pattern growth proceeds at a

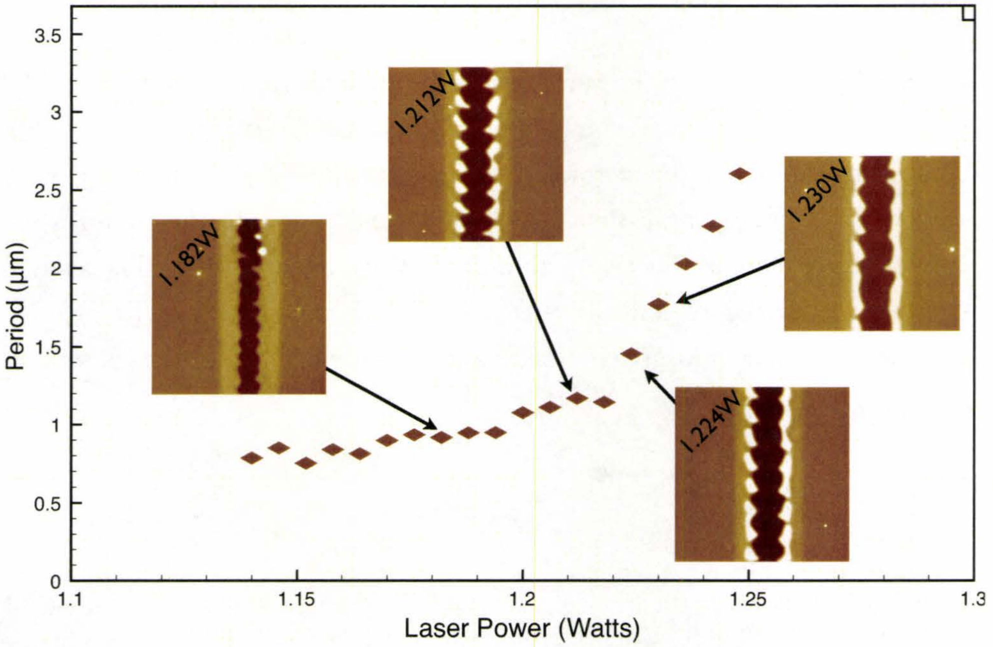

Figure 3.6: Pattern period as a function of laser power. The inset atomic force micrographs show the morphology of the indicated patterns. Note that pattern growth is more rapid once the islands begin to coalesce. This pattern was formed using a constant scan speed of 100 μm/sec on a film 34.4 nm thick.

significantly faster rate.

The increased growth rate of the patterns can be partially understood by examining the effect of the edge tension of the two islands just before and just after they come into contact with each other. As shown in figure 3.7, before contact is made, the islands have a relatively large radius of curvature everywhere, and so a low local Laplace pressure.[1] As contact is made, the islands merge, resulting in two very sharp "corners". These sharp corners have a very small radius of curvature, and so a comparatively high local pressure, which will rapidly drive the combined island to a more 'rounded' shape. Thus, the edge tension can be thought of as an elastic band stretched around the combined island, pulling it towards a shape with a large radius of curvature. This driving force can also conceivably pull material into the island from the surrounding regions, effectively aiding the Marangoni induced flow away from the central heated region. In either case, the expected growth rate of the diblock patterns could be expected to increase, which is what is observed.

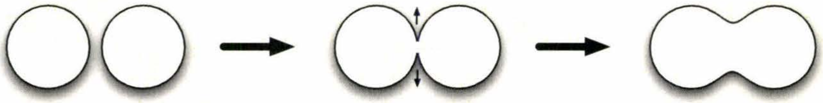

Figure 3.7: Schematic diagram of two islands merging. The islands initially have low edge tensions (left). Upon merging, the combined island has a very high edge tension near the contact point (middle). This tension causes rapid changes in the shape of the combined island (right).

Interestingly, this rate of rapid growth associated with merging island begins at a pattern period of approximately 1.1 μm. This period corresponds exactly with the period at which increased growth is observed during the scan velocity experiments (section 3.2.2). As changing either the laser power or the scan velocity will effectively change the absorbed energy, it is reasonable to conclude that changing these parameters would affect the pattern growth in similar ways.

---

[1] The change in Laplace pressure at an interface is related to the interfacial tension, γ, and the radius of curvature of the interface, R, in the following way: $\Delta p = \frac{2\gamma}{R}$. [39]

3.2.4 Film Thickness

Modifying scan speed and laser power both have the effect of changing the input power, which has been shown to impact pattern formation and growth similarly. A parameter that can be modified which does not change the input power is the thickness of the film. The experiment in section 3.2.3 was repeated for an additional 9 films, each with a different thickness. The thicknesses were measured using an atomic force microscope, and ranged from 28.6 to 43.6 nm. The combined data of period as a function of laser power for each of the 10 films is shown in figure 3.8.

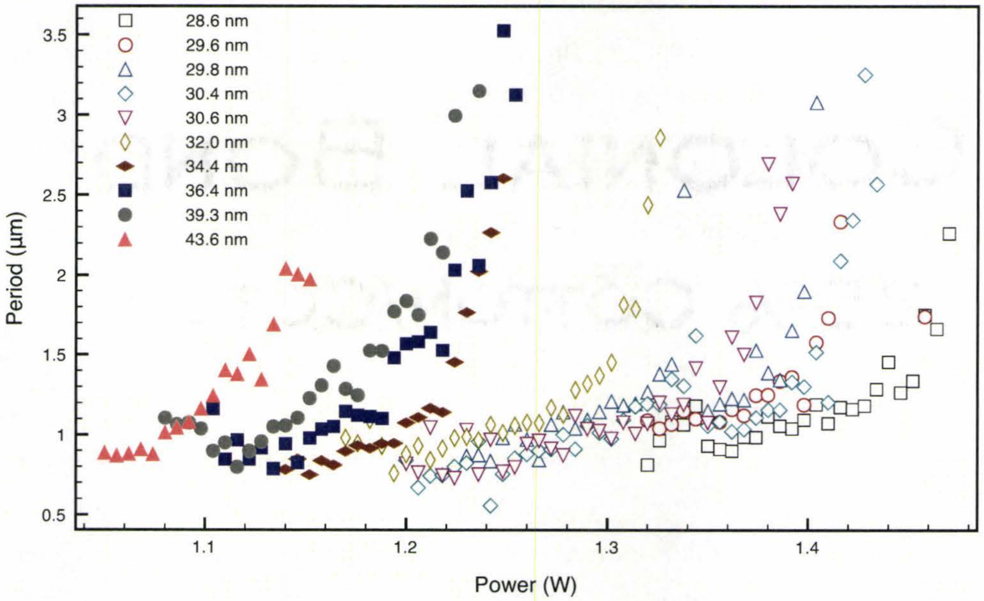

Figure 3.8: Pattern period as a function of laser power and film thickness. All patterns were formed using a constant scan speed of 100 μm/sec.

From this data, it can be seen that the relationship between period and power is qualitatively the same for each thickness. Rapid pattern growth at higher laser powers is preceded by slow growth at low powers. It is also of interest that the ~1.1 μm period threshold above which growth is accelerated is a constant feature of all of the samples. The one noticeable difference between thicknesses is an apparent shift in the required laser power needed to form a given pattern. Thin films require more power to achieve the same feature size then thicker films.

While this behavior could indicate a fundamental difference in pattern formation at different thicknesses, it must be kept in mind that thin polymer films on silicon effectively form antireflection coatings. Thus, any change in thickness would result in a change in the properties of this coating, and so a change in absorbed power. Any data obtained by changing the thickness must therefore be normalized by the resulting change in absorbed power in order to draw meaningful conclusions from it.

The reflectance of each of the 10 samples was measured by comparing the power reflected from each film to the power reflected from a bare silicon substrate. A very low laser power was used to ensure that laser lithography did not occur during these measurements. The reflectance of the films is plotted in figure 3.9. Also plotted is the expected change in reflectivity as calculated using equations 1.10 and 1.11, along with the optical properties listed in Table 1.1. The data shows that the reflectivity of the films does in fact change in a predicable way, and must be accounted for.

Re-normalizing all of the data in figure 3.8 by the reflectance shown in figure 3.9 results in the data plotted in figure 3.10. All of the slow growth regions of the line collapse onto a single master curve. This indicates that the shifts in laser power evident in the various thicknesses is due almost entirely to changes in the reflectivity of the samples. Though changing thickness does not change incident laser power, it does impact how much energy is absorbed, and so, effective laser power.

One other suggestive piece of information can be extracted from the fast growth (above ~ 1.1 μm) sections of the data in figure 3.10. From section 1.2.1, the lamellar thickness of this polymer is approximately 14.5 nm. Co-

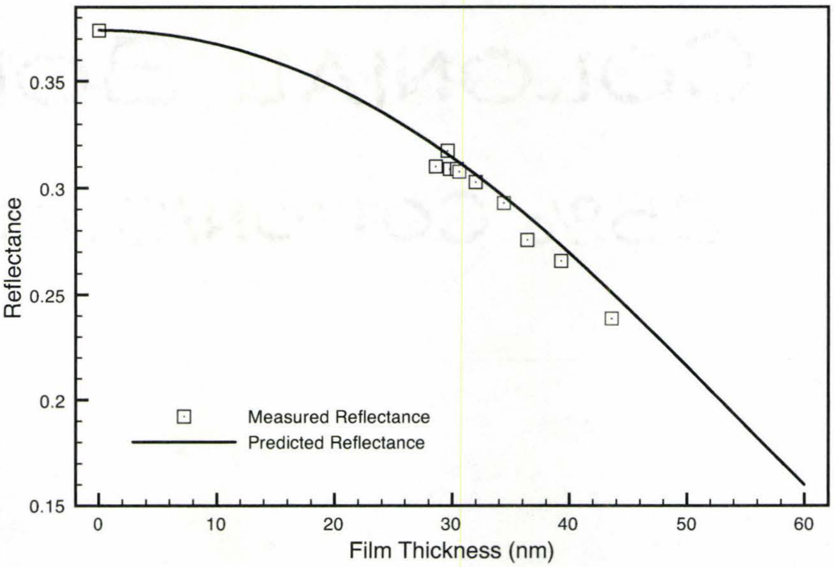

Figure 3.9: Scaled reflectivity of samples.

incidentally, the thinnest and thickest polymers measured differed by 15 nm. Interestingly, though they are the furthest distance apart in thickness, the period curves for these films lie almost directly on top of each other on the extreme right of the plot. The thicknesses that are halfway between them (differing by half of a lamellar thickness) lie on the opposite end of the plot, on the extreme left.

The fact that films that differ in height by an integer number of layers behave similarly indicates that the growth of the pattern could depend on the amount of 'excess' material above that required for a 'complete' layer. Figure 3.11 shows the position of the 'knee' between slow and fast growth regions as a function of excess thickness, scaled to lamellar height. There appears to be a periodic relationship between lamellar growth and film thickness, with the periodicity of the relationship equal to the lamellar thickness.

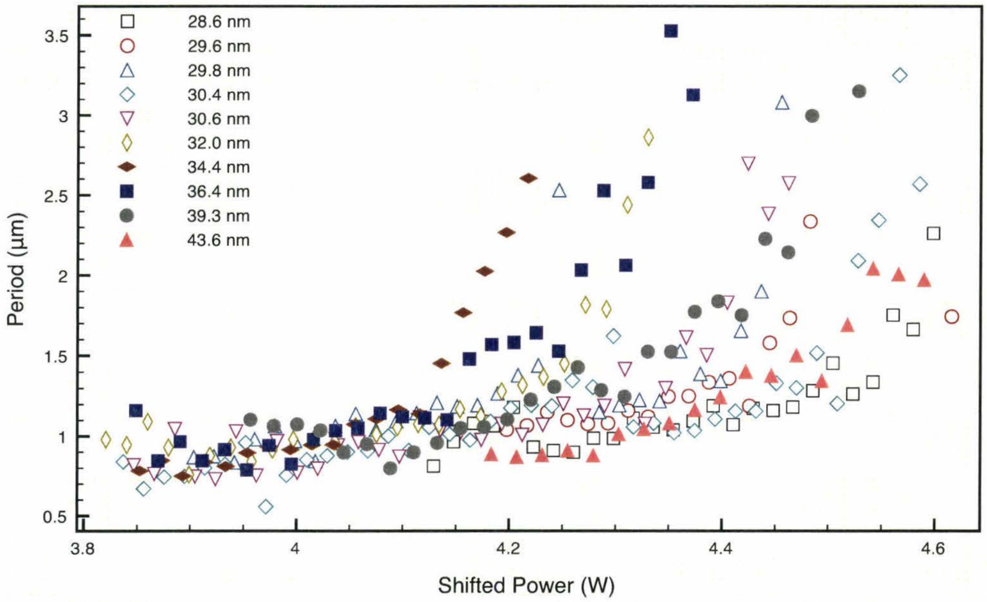

Figure 3.10: Pattern period as a function of normalized (shifted) power and thickness.

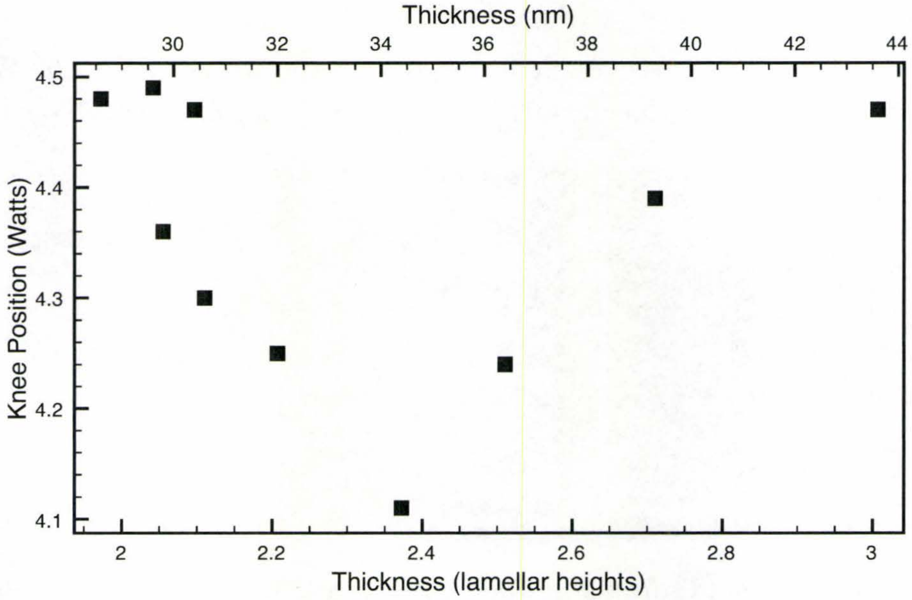

Figure 3.11: 'Knee position' as a function of scaled thickness. This plot shows the position of an identifying feature (the 'knee' between slow and fast growth regions) from each of the 10 period vs. power data sets. The scaled thickness is equal to the thickness of the thin film in number of lamellar heights (taken to be 14.5 nm).

3.2.5 Temperature

A final parameter adjusted during the laser lithography experiments was the 'ambient' temperature of the film. The film is typically held at temperature between 90 and 130 ℃ in order to keep the polymer in a melt state and facilitate the flow of material. Higher temperatures should lead to lower viscosities and more rapid pattern formation.

Figure 3.12 shows patterns produced on the same sample at a constant laser power. The same set of lines was drawn at three temperatures: 96℃, 98℃, and 100℃. In this case, the laser power output ranged from 1.00 Watts for the first (topmost) line to 1.09 W for the last (bottommost) line.

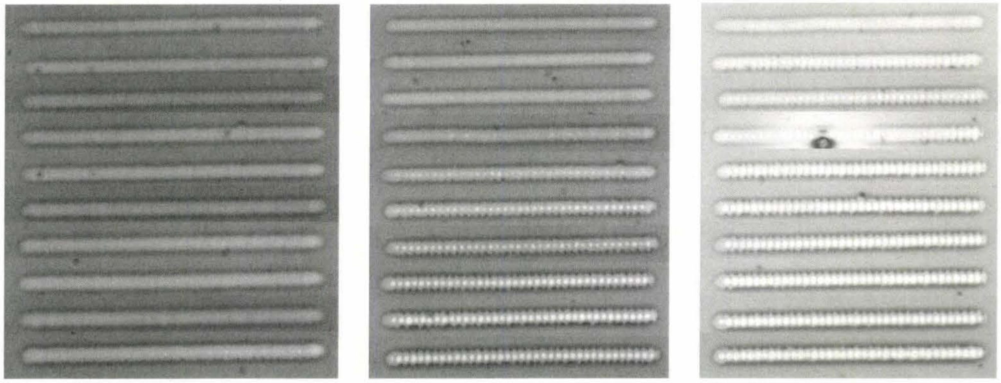

Figure 3.12: Pattern Formation at Various Powers and Temperatures - Lines drawn with increasing laser power at three different temperatures: 96℃ (left), 98℃ (centre), and 100℃ (right). Power was incremented from 1.00 to 1.09 Watts in 0.01 Watt steps. All patterns were formed at a constant scan velocity of 100 μm/sec. To ease comparison, each composite image is composed of 10 individual images of the sample that have been stitched together.

Pattern formation is obviously enhanced with increasing substrate temperature. While no patterns are visible at 96℃, they appear for most of the lines at 98℃, and for all of them at 100℃. Of greater interest is what occurs when these samples are annealed. Figure 3.13 shows the temperature profile of the anneal. Significantly, the sample is soaked at 130℃ overnight and is briefly heated to 160℃. This temperature profile would heat the entire sample to temperatures roughly equivalent to those experienced locally by the laser-heated regions. The post-annealed patterns are shown in figure 3.14.

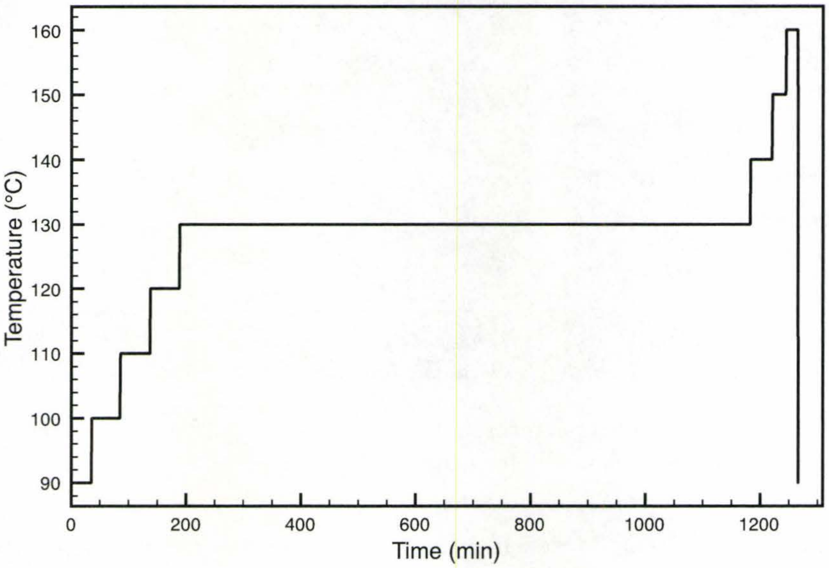

Figure 3.13: Temperature profile of the annealing step.

Of interest in the post-annealed pictures is the presence of the pattern within lines that previously showed no evidence of them. In particular, all of the lines drawn at 96°C show the pattern, whereas none of them did before the anneal. Since the Marangoni induced flow occurs only in the presence of a temperature gradient, this flow cannot be the cause of the pattern growth in these samples. *The only remaining driving force would be the tendency for the diblocks to order.* This would seem to indicate that while Marangoni induced flow is required to start pattern formation by creating a trench within the polymer, the main driving force is the ordering of the diblocks.

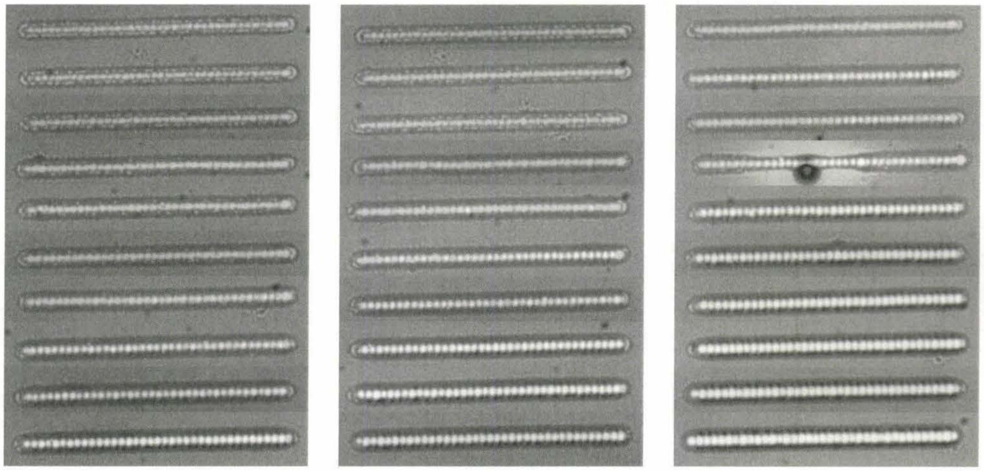

Figure 3.14: Post-anneal patterns. All lines now show evidence of patterns, including ones without such evidence before the anneal.

Further, whereas increasing laser power or decreasing scan speed sufficiently will cause the pattern to disappear by removing all material within the trench, extended annealing at elevated temperatures seems to produce self-limiting pattern growth. The size of the holes grows until their size is equal to the lateral dimensions of the trench, after which growth seems to nearly stop.

Chapter 4

Conclusions

Laser lithography has proven to be a remarkably flexible tool in patterning polymer films. By taking advantage of the ability of diblock copolymers to self assemble, its utility has been extended to include the formation of nanoscale patterns in thin polymer films. The regularity of the islands and holes that make up these these patterns, along with their extraordinarily large aspect ratios, make them particularly interesting from both a scientific and technological aspect.

By varying the parameters of film composition, scan velocity, laser power, film thickness and sample temperature, much insight has been gained into the formation and growth of the patterns. It has been shown that the pattern formation is due to the interplay between molecular ordering and the Marangoni effect, as it is not present in materials which do not self assemble. Further, several independent methods of changing the absorbed power of a given volume of material, including modifying the scan velocity, changing the laser output power, and changing the thickness of the films have all shown that pattern formation is most strongly dependent on the absorbed power. Even the variation of the patterns with film thickness can be mostly attributed to the change in reflectivity of these samples. Nevertheless, thickness does seem to play a role in that there appears to be a periodic variation in pattern growth that can be attributed to the height of the film relative to the lamellar thickness. Finally, through the annealing experiments described in section 3.2.5, it can be seen that although laser lithography is required to initiate and direct the growth of the patterns, this growth is a result of the diblock ordering process.

The investigations of this thesis have shed much light on pattern formation, though they have also left many questions open. Two main issues that can be looked into further are the actual dynamical mechanism of pattern formation, and the periodicity of pattern growth with lamellar thickness.

A look into the dynamics of pattern growth can be made, quite literally, by implementing a high resolution camera system into the laser lithography apparatus, enabling direct observation of pattern formation under various conditions. As a heating stage is already available, this would allow a much closer look at the effects of annealing the samples compared to laser lithography alone. While the laser lithography process causes both material flow and ordering, the material flow could be 'switched off' by reducing laser power and increasing sample temperature during the experiment.

The periodic dependance on thickness can be confirmed be changing the size of the diblock molecules used in the experiment. While the work done for this thesis looked at a single molecule, a symmetric 18k-b-18k poly(styrene-b-methyl methacrylate) block, changing the size of this block would change the lamellar spacing and should thus impact the periodicity of the observed behavior. Along with changing the size of the diblock, changing its symmetry would also prove to be very interesting. While a symmetric diblock is lamella-forming, as shown in figure 1.6, microphase separation of non-symmetric blocks can result in cylindrical or spherical domains. The impact of laser lithography on these materials would be a very interesting topic of study.

During the course of this thesis, a novel patterning of diblock copolymer thin films was discovered. Subsequent experiments proved that the pattern is a result of the self assembly of diblock copolymers combined with the Marangoni effect. Though we have strong indications from these experiments that the geometry of the pattern is dependent on the geometry of the film, a full understanding of this phenomenon remains elusive. As interest in using diblock copolymers to create patterns is stimulated by a continued drive in nanotechnology, it becomes increasingly important to have an understanding of these types of patterns and the dynamics of their formation. In this regard, laser lithography seems ideally positioned to continue the exploration of this emerging field of study.

Bibliography

[1] Marc J. Madou. *Fundamentals of Microfabrication.* CRC Press, Boca Raton, FL, 2nd edition, 2002.

[2] James D. Plummer, Michael D. Deal, and Peter B. Griffin. *Silicon VLSI Technology.* Prentice Hall, Upper Saddle River, New Jersey 07458, 2000.

[3] D Bratton, D Yang, JY Dai, and CK Ober. Recent progress in high resolution lithography. *Polymers For Advanced Technologies*, 17:94–103, 2006.

[4] Wei Lu and Ann Marie Sastry. Self-assembly for semiconductor industry. *IEEE Transactions On Semiconductor Manufacturing*, 20:421–431, 2007.

[5] Masao Doi. *Inroduction to Polymer Physics.* Oxford University Press, New York, 1995.

[6] Nikos Hadjichristidis, Stergios Pispas, and George A. Floudas. *Block Copolymers : Synthetic Strategies, Physical Properties and Applications.* John Wiley & Sons Inc, New Jersey, 2003.

[7] MW Matsen. The standard gaussian model for block copolymer melts. *Journal of Physics-Condensed Matter*, 14:R21–R47, 2002.

[8] Richard A.L. Jones. *Soft Condensed Matter.* Oxford University Press, 2002.

[9] Ian W. Hamley. *The Physics of Block Copolymers.* Oxford University Press, New York, 1998.

[10] AN Semenov. Contribution to the theory of microphase layering in block-copolymer melts. *Zhurnal Eksperimentalnoi I Teoreticheskoi Fiziki*, 88:1242–1256, 1985.

[11] FS Bates and GH Fredrickson. Block copolymer thermodynamics - theory and experiment. *Annual Review of Physical Chemistry*, 41:525–557, 1990.

[12] AN Semenov. Theory of block-copolymer interfaces in the strong segregation limit. *Macromolecules*, 26:6617–6621, 1993.

[13] TP Russell, RP Hjelm, and PA Seeger. Temperature dependence of the interaction parameter of polystyrene and poly(methyl methacrylate). *Macromolecules*, 23:890–893, 1990.

[14] Easan Sivaniah, Shinya Matsubara, Yue Zhao, Takeji Hashimoto, Kenji Fukunaga, Edward J. Kramer, and Tom E. Mates. Symmetric diblock copolymer thin films on rough substrates: Microdomain periodicity in pure and blended films. *Macromolecules*, 41:2584–2592, 2008.

[15] MW Matsen and FS Bates. Unifying weak- and strong-segregation block copolymer theories, 1996.

[16] Frank L. Pedrotti and Leno S. Pedrotti. *Introduction to Optics*. Prentice Hall, Upper Saddle River, New Jersey 07458, 1993.

[17] Edward D. Palik, editor. *Handbook of Optical Constants of Solids*. Academic Press Inc., Orlando, Florida, 1985.

[18] J. Brandrup, E.H. Immergut, and E.A. Grulke, editors. *Polymer Handbook*. John Wiley & Sons Inc, New York, NY, fourth edition, 1999.

[19] John M. Hudson. Laser lithography of thin polymer films. Master's thesis, McMaster University, 2004.

[20] S Wu. Surface and interfacial tensions of polymer melts. ii. poly(methyl methacrylate), poly(n-butyl methacrylate), and polystyrene. *The Journal of Physical Chemistry*, 74(3):632, 1970.

[21] Polymer Source Inc. Website. `http://www.polymersource.com/shoppingCart/product.asp?ID=408`.

[22] BD Washo. Rheology and modeling of spin coating process. *IBM Journal of Research and Development*, 21:190–198, 1977.

[23] WW Flack, DS Soong, AT Bell, and DW Hess. A mathematical-model for spin coating of polymer resists. *Journal of Applied Physics*, 56:1199–1206, 1984.

[24] SA Jenekhe and SB Schuldt. Coating flow of non-newtonian fluids on a flat rotating-disk. *Industrial and Engineering Chemistry Fundamentals*, 23:432–436, 1984.

[25] KJ Ruschak. Coating flows. *Annual Review of Fluid Mechanics*, 17:65–89, 1985.

[26] SJ Weinstein and KJ Ruschak. Coating flows. *Annual Review of Fluid Mechanics*, 36:29–53, 2004.

[27] J. Ashmore, A. Q. Shen, H. P. Kavehpour, H. A. Stone, and G. H. McKinley. Coating flows of non-newtonian fluids: weakly and strongly elastic limits. *Journal of Engineering Mathematics*, 60:17–41, 2008.

[28] CM Stafford, KE Roskov, TH Epps, and MJ Fasolka. Generating thickness gradients of thin polymer films via flow coating. *Review of Scientific Instruments*, 77, 2006.

[29] AP Smith, JF Douglas, JC Meredith, EJ Amis, and A Karim. High-throughput characterization of pattern formation in symmetric diblock copolymer films. *Journal of Polymer Science Part B-Polymer Physics*, 39:2141–2158, 2001.

[30] AP Smith, JF Douglas, JC Meredith, EJ Amis, and A Karim. Combinatorial study of surface pattern formation in thin block copolymer films. *Physical Review Letters*, 87, 2001.

[31] Coherent Laser Group. *Operator's Manual, Verdi V-2/V-5 Diode Pumped Lasers.*

[32] Coherent Inc. Coherent comparison chart. Website. `http://www.coherent.com/Lasers/index.cfm?fuseaction=popups.ShowAttributes&ID=873`.

[33] Newport Corporation. Laser line polarizing cube beamsplitters. Website. `http://www.newport.com/store/genproduct.aspx?id=141124&lang=1033&Section=Spec`.

[34] Newport Corporation. Electronic shutter system. Website. `http://www.newport.com/store/genproduct.aspx?id=579081&lang=1033&Section=Pricing`.

[35] Nobelprize.org. Physics 1986. Website. `http://nobelprize.org/nobel_prizes/physics/laureates/1986/`.

[36] Milton Ohring. *Materials Science of Thin Films: Deposition and Structure.* Academic Press, San Diego, CA, 2002.

[37] *diCaliber Instrument Operations Manual.* Veeco Instruments Inc., 2006.

[38] Dawn Bonnell, editor. *Scanning Probe Microscopy and Spectroscopy.* Wiley-VCH, Inc., New York, NY, second edition, 2001.

[39] Pierre-Gilles de Gennes, Françoise Brochard-Wyart, and David Quéré. *Capillarity and Wetting Phenomena.* Springer, New York, 2003.

Appendices

Appendix A

Laser Specifications

Table A.1: Laser Specifications

Parameter	Value
Maximum Power	2.2 Watts
Wavelength	532 nm
Linewidth	<5 MHz
Beam Diameter	2.25 mm ± 10%
Beam Divergence	<0.5 mrad
M^2 Factor	<1.1
Pointing Stability	2 μrad/℃
Power Stability	±1%
Noise	<0.03% rms
Polarization	vertical, >100:1

Appendix B

Spot Size Calculation

The minimum focused spot size of the laser beam, d, can be calculated if the focal length of the lens, f, and the divergence of the laser beam, ϕ is known. The divergence for a laser beam depends on the wavelength of the light being emitted, λ, and the diameter of the laser beam at its waist, D, according to the following equation:

$$\phi = \frac{1.27\lambda}{D} \tag{B.1}$$

Using 532 nm as the operating wavelength and 2.25 mm as the beam diameter (from Appendix A), the divergence of the beam is calculated to be 0.300 mrad.

The minimum spot size d can now be estimated using the relationship:

$$d \approx f\phi \tag{B.2}$$

Taking f as the focal length of the objective (20.0 mm), we calculate the minimum spot size to be 6.00 μm.

Appendix C

Backlash Correction Algorithm

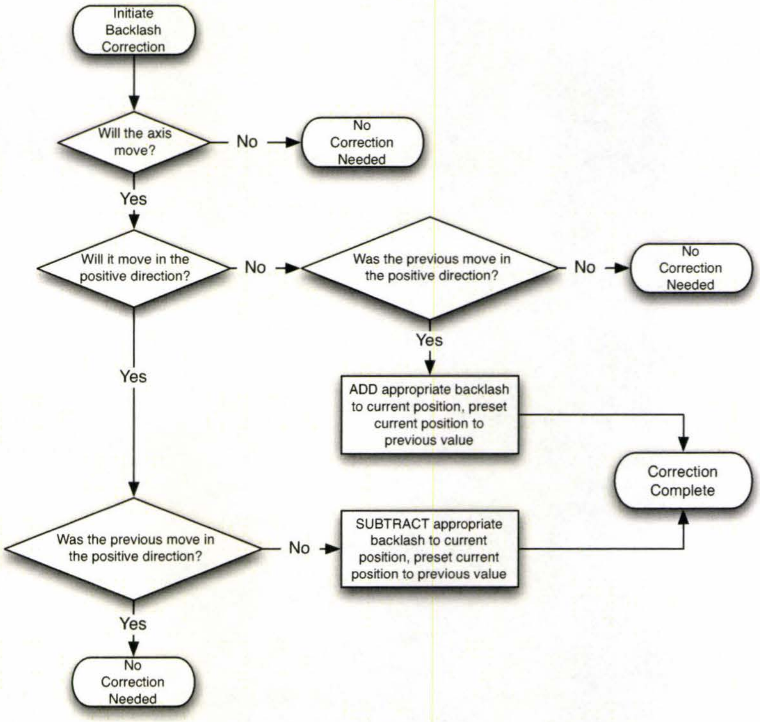
Initiate Backlash Correction
Will the axis move?
No
No Correction Needed
Yes
Will it move in the positive direction?
No
Was the previous move in the positive direction?
No
No Correction Needed
Yes
ADD appropriate backlash to current position, preset current position to previous value
Yes
Correction Complete
Was the previous move in the positive direction?
No
SUBTRACT appropriate backlash to current position, preset current position to previous value
Yes
No Correction Needed

Figure C.1: Flow Diagram of the Backlash Correcting Routine

9072-104